Restoration of replication fork stability in BRCA1- and BRCA2-deficient cells by inactivation of SNF2-family fork remodelers

Postprint (Author accepted manuscript)

Taglialatela, Angelo; Department of Genetics and Development, Columbia University Medical Center, New York (NY), USA - Herbert Irving Comprehensive Cancer Center, Columbia University Medical Center, New York (NY), USA

Alvarez, Silvia; Department of Genetics and Development, Columbia University Medical Center, New York (NY), USA - Herbert Irving Comprehensive Cancer Center, Columbia University Medical Center, New York (NY), USA

Leuzzi, Giuseppe; Department of Genetics and Development, Columbia University Medical Center, New York (NY), USA - Herbert Irving Comprehensive Cancer Center, Columbia University Medical Center, New York (NY), USA

Sannino, Vincenzo; DNA metabolism laboratory, IFOM, FIRC Institute for Molecular Oncology, Milan, Italy

Ranjha, Lepakshi; Institute for Research in Biomedicine (IRB), Faculty of Biomedical Sciences, Università della Svizzera italiana, Switzerland

Huang, Jen-Wei; Department of Genetics and Development, Columbia University Medical Center, New York (NY), USA - Herbert Irving Comprehensive Cancer Center, Columbia University Medical Center, New York (NY), USA

Madubata, Chioma; Department of Systems Biology, Columbia University Medical Center, New York (NY), USA - Department of Biomedical Informatics, Columbia University Medical Center, New York (NY), USA

Anand, Roopesh; Institute for Research in Biomedicine (IRB), Faculty of Biomedical Sciences, Università della Svizzera italiana, Switzerland

Levy, Brynn; Department of Pathology and Cell Biology, Columbia University Medical Center, New York (NY), USA

Rabadan, Raul; Department of Systems Biology, Columbia University Medical Center, New York (NY), USA - Department of Biomedical Informatics, Columbia University Medical Center, New York (NY), USA

Cejka, Petr; Institute for Research in Biomedicine (IRB), Faculty of Biomedical Sciences, Università della Svizzera italiana, Switzerland - Institute of Biochemistry, Department of Biology, ETH Zurich, Switzerland

Costanzo, Vincenzo; DNA metabolism laboratory, IFOM, FIRC Institute for Molecular Oncology, Milan, Italy

Ciccia, Alberto; Department of Genetics and Development, Columbia University Medical Center, New York (NY), USA - Herbert Irving Comprehensive Cancer Center, Columbia University Medical Center, New York (NY), USA

Originally published in:

Molecular Cell

2017 / Vol. 68 / n. 2 (19 October) / pp. 414-430.e8

Published version: https://doi.org/10.1016/j.molcel.2017.09.036

Online publication: 2017-10-19

Restoration of replication fork stability in BRCA1- and BRCA2-deficient cells by inactivation of SNF2-family fork remodelers

Angelo Taglialatela[1,2,9], **Silvia Alvarez**[1,2,9], **Giuseppe Leuzzi**[1,2,10], **Vincenzo Sannino**[3,10], **Lepakshi Ranjha**[4,10], **Jen-Wei Huang**[1,2,10], **Chioma Madubata**[5,6], **Roopesh Anand**[4], **Brynn Levy**[7], **Raul Rabadan**[5,6], **Petr Cejka**[4,8], **Vincenzo Costanzo**[3], and **Alberto Ciccia**[1,2,11,*]

[1]Department of Genetics and Development, Columbia University Medical Center, New York, NY 10032, USA [2]Herbert Irving Comprehensive Cancer Center, Columbia University Medical Center, New York, NY 10032, USA [3]DNA metabolism laboratory, IFOM, FIRC Institute for Molecular Oncology, 20139 Milan, Italy [4]Institute for Research in Biomedicine, Universita' della Svizzera italiana, 6500 Bellinzona, Switzerland [5]Department of Systems Biology, Columbia University Medical Center, New York, NY 10032, USA [6]Department of Biomedical Informatics, Columbia University Medical Center, New York, NY 10032, USA [7]Department of Pathology and Cell Biology, Columbia University Medical Center, New York, NY 10032, USA [8]Department of Biology, Institute of Biochemistry, Swiss Federal Institute of Technology, 8093 Zurich, Switzerland

SUMMARY

To ensure the completion of DNA replication and maintenance of genome integrity, DNA repair factors protect stalled replication forks upon replication stress. Previous studies have identified a critical role for the tumor suppressors BRCA1 and BRCA2 in preventing the degradation of nascent DNA by the MRE11 nuclease after replication stress. Here we show that depletion of SMARCAL1, a SNF2-family DNA translocase that remodels stalled forks, restores replication fork stability and reduces the formation of replication stress-induced DNA breaks and chromosomal aberrations in BRCA1/2-deficient cells. In addition to SMARCAL1, other SNF2-family fork remodelers, including ZRANB3 and HLTF, cause nascent DNA degradation and genomic instability in BRCA1/2-deficient cells upon replication stress. Our observations indicate that nascent DNA degradation in BRCA1/2-deficient cells occurs as a consequence of MRE11-

[*]Correspondence: ac3685@cumc.columbia.edu.
[9]These authors contributed equally
[10]These authors contributed equally
[11]Lead contact

SUPPLEMENTAL INFORMATION
Supplemental Information includes 7 supplemental figures and one supplemental table.

AUTHOR CONTRIBUTIONS
A.T., S.A. and A.C. conceived the study. A.T., S.A., G.L. and J.W.H. executed the experimental work under the supervision of A.C. V.S. conducted the electron microscopy studies under the supervision of V.C. and L.R. performed the in vitro biochemical assays under the supervision of P.C. C.M. performed the patient survival analyses under the supervision of R.R. R.A. provided recombinant MR and MRN proteins for in vitro assays. B.L. helped with the analysis of chromosomal aberrations. A.T., S.A. and A.C. wrote the manuscript.

dependent nucleolytic processing of reversed forks generated by fork remodelers. These studies provide mechanistic insights into the processes that cause genome instability in BRCA1/2-deficient cells.

IN BRIEF

Taglialatela et al. report that the replication fork remodelers SMARCAL1, ZRANB3 and HLTF promote the degradation of nascent DNA catalyzed by the MRE11 nuclease in BRCA1/2-deficient mammary epithelial cells treated with replication stress-inducing agents. Depletion of fork remodelers restores fork integrity and reduces genome instability in BRCA1/2-deficient cells.

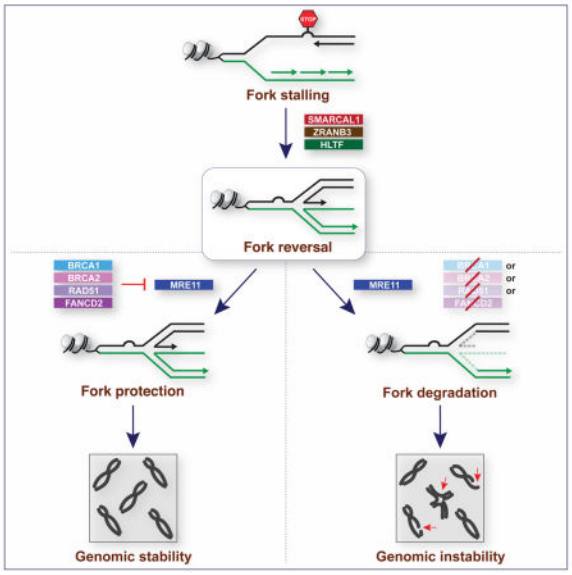

Keywords

DNA replication stress; replication fork instability; replication fork reversal; BRCA1 and BRCA2; RAD51; SMARCAL1; ZRANB3; HLTF; MRE11; breast and ovarian cancer

INTRODUCTION

Germline *BRCA1* and *BRCA2* mutations are highly penetrant, predisposing 20–80% of carriers to breast and/or ovarian cancer (Apostolou and Fostira, 2013). BRCA1 and BRCA2 are central components of the DNA damage response that preserve genome integrity by regulating multiple steps of homology-directed repair (HDR) of DNA double-strand breaks (DSBs), including the nucleolytic processing of DSBs and the assembly of the RAD51 recombinase onto resected DSB ends (Prakash et al., 2015). BRCA1/2 also possess HDR-independent functions that promote genome integrity. Earlier work had established that BRCA2 is required for the stabilization of stalled replication forks generated upon treatment with the ribonucleotide reductase inhibitor hydroxyurea (HU) (Lomonosov et al., 2003), while more recent studies have shown that the nascent DNA strands of HU-induced stalled replication forks undergo extensive nucleolytic degradation in BRCA2-deficient cells (Schlacher et al., 2011). Importantly, Schlacher et al. reported that BRCA2 protects stalled

forks in an HDR-independent but RAD51-dependent manner (Schlacher et al., 2011), confirming previous work that uncovered nascent DNA degradation in *Xenopus laevis* egg extracts depleted of RAD51 (Hashimoto et al., 2010). Fork protection also depends on BRCA1 and components of the Fanconi anemia (FA) pathway, which cooperate with BRCA2 and RAD51 in preventing nascent DNA degradation (Schlacher et al., 2012). Nascent DNA degradation in BRCA1/2-deficient cells and in RAD51-depleted *X. laevis* egg extracts is mediated by the MRE11 nuclease (Hashimoto et al., 2010; Schlacher et al., 2011; Schlacher et al., 2012), whose recruitment to stalled forks is regulated by the poly(ADP-ribose) polymerase PARP1, the chromatin remodeler CHD4, the histone methyltransferase MLL3/4 and its interactor PTIP (Ding et al., 2016; Ray Chaudhuri et al., 2016). Despite these important findings, the precise mechanisms by which BRCA1/2 protect stalled forks from degradation upon replication stress remain to be determined.

Replication stress induces the reversal of stalled replication forks into four-way structures in which the two nascent DNA strands anneal to form a fourth arm (Neelsen and Lopes, 2015). The reversal of stalled forks can allow DNA synthesis to pause and resume once the block has been relieved or, if the block cannot be removed, to bypass it by using the complementary nascent DNA strand as a template (Neelsen and Lopes, 2015). Several enzymes have been shown to exhibit fork reversal activity, including the DNA helicases FBH1, BLM, WRN and RECQL5 and the DNA translocases RAD54, FANCM, HLTF, SMARCAL1 and ZRANB3 (Betous et al., 2013; Betous et al., 2012; Blastyak et al., 2010; Ciccia et al., 2012; Kile et al., 2015; Neelsen and Lopes, 2015). SMARCAL1, ZRANB3 and HLTF are SNF2-family members that catalyze fork remodeling by similar mechanisms of action (Achar et al., 2015; Badu-Nkansah et al., 2016; Betous et al., 2013; Betous et al., 2012; Blastyak et al., 2010; Ciccia et al., 2012; Kile et al., 2015). SMARCAL1 and ZRANB3 are recruited to sites of replication fork stalling by the ssDNA-binding complex RPA and the polyubiquitinated form of the DNA polymerase clamp PCNA, respectively (Bansbach et al., 2009; Ciccia et al., 2009; Ciccia et al., 2012; Postow et al., 2009; Weston et al., 2012; Yuan et al., 2009, 2012; Yusufzai et al., 2009). PCNA polyubiquitination is mediated by HLTF, which possesses both ubiquitin ligase and fork-remodeling activities (Unk et al., 2010). In agreement with a key role for SMARCAL1, ZRANB3 and HLTF in replication fork metabolism, RNAi-mediated depletion of these factors decreases the efficiency of replication fork restart upon replication stress (Blastyak et al., 2010; Ciccia et al., 2009; Ciccia et al., 2012; Yuan et al., 2012). These studies suggest that SMARCAL1, ZRANB3 and HLTF play central functions in fork remodeling upon replication stress.

In this study we report that depletion of SMARCAL1, ZRANB3 or HLTF protects stalled forks from MRE11-dependent degradation in BRCA1/2-deficient mammary epithelial cells. By using complementation assays, we show that the fork-remodeling activities of the above enzymes are required for inducing nascent DNA degradation in BRCA1/2-deficient cells. Using electron microscopy and in vitro biochemical assays, we additionally demonstrate that reversed forks generated by SNF2-family fork remodelers are nucleolytically processed by MRE11, thus resulting in nascent DNA degradation in BRCA1/2-deficient cells. Depletion of fork remodelers reduces replication stress-induced DNA damage and chromosomal aberrations in BRCA1/2-deficient cells, suggesting that genomic instability can be alleviated in BRCA1/2-deficient cells by inhibiting fork remodeling. These studies provide

mechanistic insights into the underlying causes of genomic instability in BRCA1/2-deficient cells.

RESULTS

SMARCAL1 depletion prevents nascent DNA degradation in BRCA1/2-deficient cells upon replication stress

Previous studies suggest that the nascent DNA degradation observed in BRCA1/2-deficient cells in response to HU treatment depends on the formation of reversed fork intermediates (Schlacher et al., 2011; Schlacher et al., 2012). Given the central role of SMARCAL1 in fork reversal (Betous et al., 2012; Ciccia et al., 2012), we reasoned that SMARCAL1 might render stalled forks susceptible to nucleolytic degradation in BRCA1/2-deficient cells. To test this hypothesis, we monitored nascent DNA degradation on single DNA fibers in MCF10A cells subjected to shRNA-mediated depletion of SMARCAL1, BRCA1 and/or BRCA2 (Figure 1A). To this end, MCF10A cells were subjected to two sequential pulses with the nucleotide analogs chlorodeoxyuridine (CIdU, red) and iododeoxyuridine (IdU, green) and DNA replication was subsequently arrested for 5 hrs with 2 mM HU (Figure 1B). Fork degradation was then assessed by measuring the ratio of IdU to CldU tract lengths in response to HU (Figure 1C). As expected (Schlacher et al., 2011; Schlacher et al., 2012), depletion of BRCA1 or BRCA2 significantly reduced the ldU/CldU median tract length in HU-treated cells compared to control cells (Figure 1B–C), confirming that upon fork stalling the most recently synthesized DNA of the nascent strands (i.e., IdU labeled) is degraded in BRCA1/2-deficient cells. Remarkably, this reduction in ldU/CldU median tract length was abolished upon co-depletion of SMARCAL1 with two independent shRNAs, indicating that the nascent DNA degradation caused by BRCA1/2 deficiency is dependent on SMARCAL1 (Figure 1B–C). Similarly, SMARCAL1 depletion abolished the reduction in ldU/CldU median tract length observed in BRCA1-depleted cells upon a 5 hr treatment with the topoisomerase I inhibitor camptothecin (CPT) (Figure S1A). These results indicate that SMARCAL1 promotes nascent DNA degradation in BRCA1/2-deficient cells in response to replication stress.

Inhibition of the nuclease activity of MRE11 with mirin has been shown to prevent nascent DNA degradation in BRCA1/2-deficient cells (Schlacher et al., 2011; Schlacher et al., 2012). In agreement with these findings, we observed that mirin treatment prevented the reduction in ldU/CldU median tract length in HU-treated MCF10A cells depleted of BRCA1/2 (Figure 1C). Interestingly, SMARCAL1 depletion decreased nascent DNA degradation in BRCA1/2-deficient cells to a similar extent as mirin treatment (Figure 1C). Together, these data suggest that SMARCAL1 depletion prevents MRE11-dependent nascent DNA degradation in HU-treated BRCA1/2-deficient cells.

SMARCAL1 depletion prevents nascent DNA degradation induced by FANCD2 deficiency or RAD51 inhibition

BRCA1 and BRCA2 cooperate with the FA pathway to maintain replication fork stability upon replication stress (Schlacher et al., 2012). To determine whether the nascent DNA degradation observed in FA-deficient cells is dependent on SMARCAL1, we depleted

SMARCAL1 in FANCD2-deficient PD20 cells (Figure S1B) and subjected these cells to DNA fiber analysis. In line with previous studies (Schlacher et al., 2012), PD20 cells exhibited HU-induced nascent DNA degradation, which was abolished upon FANCD2 re-expression (Figure 1D). Remarkably, SMARCAL1 depletion prevented nascent DNA degradation in PD20 cells, indicating that SMARCAL1 promotes fork instability in FA-deficient cells (Figure 1D).

BRCA1 and BRCA2 are required for the assembly of RAD51 filaments onto ssDNA, which are subsequently stabilized by FANCD2 and other DNA repair factors (Prakash et al., 2015; Sato et al., 2016). RAD51 is known to play a critical role in preventing MRE11-dependent degradation of nascent DNA and its overexpression suppresses fork instability in BRCA2- or FANCD2-deficient cells (Hashimoto et al., 2010; Schlacher et al., 2011; Schlacher et al., 2012). Recent high-throughput screens have identified the small molecule B02 as an inhibitor of the DNA-binding and strand exchange activities of RAD51 (Huang et al., 2012). To test whether RAD51 inhibition causes SMARCAL1-dependent nascent DNA degradation, MCF10A cells were treated with HU in combination with B02 (Figure 1E). In agreement with previous studies (Leuzzi et al., 2016), B02 treatment caused nascent DNA degradation in HU-treated cells (Figure 1E). Notably, the reduction in ldU/CldU tract length caused by B02 in HU-treated MCF10A cells was abolished by depleting SMARCAL1 (Figure 1E). These observations indicate that SMARCAL1 promotes nascent DNA degradation under conditions that impair RAD51 binding to stalled forks.

The ATPase and RPA-binding activities of SMARCAL1 are required to promote MRE11-dependent nascent DNA degradation in BRCA1-deficient cells

SMARCAL1 is recruited by the RPA complex to stalled forks, where it promotes fork remodeling in a manner dependent on the ATPase activity of its SNF2 domain (Bansbach et al., 2009; Betous et al., 2013; Betous et al., 2012; Ciccia et al., 2009; Ciccia et al., 2012; Postow et al., 2009; Yuan et al., 2009; Yusufzai et al., 2009). To ascertain which SMARCAL1 activities are required for fork degradation in BRCA1-deficient cells, SMARCAL1 knock-out (KO) MCF10A cells generated by CRISPR-Cas9 technology were reconstituted with cDNAs encoding either wild-type (WT) or ATPase-defective (R764Q) forms of SMARCAL1 (Ciccia et al., 2009) (Figure S1C). SMARCAL1 KO cells were additionally complemented with a SMARCAL1 mutant deleted of the N-terminal 115 amino acids of SMARCAL1 ($\Delta N_{1\text{-}115}$), which are necessary and sufficient to promote RPA binding (Bansbach et al., 2009) (Figure S1C–D). As shown in Figure 1F–G, expression of WT, but not R764Q- or $\Delta N_{1\text{-}115}$-mutant, SMARCAL1 restored nascent DNA degradation in these cells upon BRCA1 depletion and HU treatment. In agreement with these findings, SMARCAL1-deficient cells from a Schimke immuno-osseous dysplasia patient (SD31) that were complemented with WT, but not ATPase-mutant (R586W) (Ciccia et al., 2009), SMARCAL1 displayed HU-induced nascent DNA degradation after siRNA-mediated BRCA1 depletion (Figure S1E–H). These observations indicate that the ATPase and RPA-binding activities of SMARCAL1 are required for nascent DNA degradation in BRCA1-deficient cells after replication stress.

SMARCAL1 promotes the formation of ssDNA gaps at replication forks in BRCA1-deficient cells

To measure at high resolution the extent of replication stress-induced degradation of nascent DNA occurring in BRCA1-deficient MCF10A cells, we visualized by electron microscopy replication intermediates (RIs) generated in the above cells in response to HU treatment. As shown in Figure 2, BRCA1 depletion caused the accumulation of RIs containing ssDNA gaps longer than 100 nucleotides (nts), including DNA replication bubbles with ssDNA regions longer than 2,000 nts (Figures 2A–C and S2A–B). As a confirmation that ssDNA gaps longer than 100 nts occur as a result of MRE11-dependent DNA degradation, mirin treatment of BRCA1-deficient cells led to a 1.6–1.8 fold reduction in the percentage of RIs with ssDNA gaps of 100–300 nts or longer than 300 nts (Figures 2B and S2A). Notably, BRCA1/SMARCAL1 co-depleted cells displayed a 2.6-fold reduction in the number of RIs with ssDNA regions longer than 300 nts compared to BRCA1-deficient cells (Figures 2B and S2A–B). Similar results were obtained in a duplicate experiment, even when considering a lower number of randomly sampled RIs, supporting the robustness of our findings (Figure S2A). These data indicate that SMARCAL1 is required for the formation of large ssDNA gaps at stalled forks in BRCA1-deficient cells.

Depletion of SMARCAL1 does not restore homology-directed repair of DNA double-strand breaks in BRCA1-deficient cells

BRCA1-deficient cells are defective in RAD51-dependent DSB repair by HDR (Prakash et al., 2015). To determine whether re-establishment of fork stability in BRCA1-deficient cells induced by SMARCAL1 depletion is accompanied by restoration of homology-directed DSB repair, BRCA1- and/or SMARCAL1-depleted MCF10A cells were subjected to ionizing radiation (IR) and immunofluorescence microscopy was then used to quantitate the percentage of cells that displayed IR-induced RAD51 nuclear foci, which reflect the formation of the RAD51 nucleoprotein filaments necessary for HDR. As expected, BRCA1 depletion reduced the number of RAD51-positive cells upon IR treatment (Figure S2C–D). However, depletion of SMARCAL1 in BRCA1-deficient cells did not alter the number of IR-induced RAD51-positive cells, suggesting that HDR-dependent DSB repair was not restored in BRCA1-deficient cells by depletion of SMARCAL1 (Figure S2C–D).

Depletion of ZRANB3 or HLTF restores replication fork stability in BRCA1/2-deficient cells in response to replication stress

The SNF2-family DNA translocases ZRANB3 and HLTF exhibit fork-remodeling activities similar to SMARCAL1 (Betous et al., 2013; Blastyak et al., 2010; Ciccia et al., 2012; Kile et al., 2015). To determine whether ZRANB3, like SMARCAL1, is required for nascent DNA degradation in BRCA1/2-deficient cells after replication stress, we depleted ZRANB3 in BRCA1/2-deficient cells using two independent shRNAs and conducted DNA fiber assays upon HU treatment, as described above (Figures 3A–B and S3A). As shown in Figure 3A–B, ZRANB3 depletion abolished the reduction in ldU/CldU median tract length caused by BRCA1/2-deficiency in a manner comparable to mirin treatment, indicating that ZRANB3 promotes MRE11-dependent nascent DNA degradation in BRCA1/2-deficient cells. Likewise, the ldU/CldU median tract length was also restored in BRCA1/2-deficient

MCF10A cells by depleting HLTF (Figures 3C–D and S3B). Distinct from ZRANB3 and HLTF, the RECQL5 helicase was not required to promote nascent DNA degradation in BRCA1-deficient cells (Figure S3C–D). These findings indicate that, in addition to SMARCAL1, ZRANB3 and HLTF are also required to promote MRE11-dependent nascent DNA degradation in BRCA1/2-deficient cells.

ZRANB3 associates with polyubiquitinated PCNA at stalled forks, where it promotes fork remodeling (Ciccia et al., 2012). To determine which activities of ZRANB3 are required to promote nascent DNA degradation in BRCA1/2-deficient cells, we complemented BRCA1/ZRANB3 co-depleted cells with WT ZRANB3 or ZRANB3 mutants defective in ATP-dependent fork-remodeling activity (K163D), association with PCNA (PIP+APIM) or binding to its polyubiquitinated form (NZF_{-zinc}) (Figure S3E–F) (Badu-Nkansah et al., 2016; Ciccia et al., 2012). As shown in Figure 3E, nascent DNA degradation was restored by expressing WT, but not K163D-, PIP+APIM- or NZF_{-zinc}-mutant, ZRANB3, indicating that the fork-remodeling and polyubiquitinated PCNA-binding activities of ZRANB3 are necessary to promote nascent DNA degradation in BRCA1-deficient cells. Similar complementation studies revealed that the HIRAN motif of HLTF, a DNA-binding domain required for HLTF-mediated fork reversal (Achar et al., 2015; Kile et al., 2015), is necessary for HLTF-dependent nascent DNA degradation in BRCA1-deficient cells (Figures 3F and S3G). These studies indicate that fork degradation in BRCA1-deficient cells depends on the fork-remodeling activities of both ZRANB3 and HLTF.

SNF2-family fork remodelers do not associate with the MRE11-RAD50-NBS1 (MRN) complex

The above observations suggest that SNF2-family DNA translocases promote MRE11-dependent nascent DNA degradation in BRCA1/2-deficient cells. To determine whether SMARCAL1, ZRANB3 and HLTF physically interact with the MRN complex to promote MRE11-dependent nascent DNA degradation, we exogenously expressed HA-tagged MRE11 and NBS1 proteins in HEK293T cells and immunoprecipitated MRE11 and NBS1 protein complexes using anti-HA beads with or without HU treatment. As shown in Figure S4A, SMARCAL1, ZRANB3 and HLTF were not detected in MRE11- or NBS1-immunoprecipates. In agreement with these findings, MRE11 and NBS1 were not identified as part of SMARCAL1 or ZRANB3 protein complexes immunoprecipitated from HEK293T cells under the above conditions (Figure S4A). Taken together, these observations indicate that SMARCAL1, ZRANB3 and HLTF do not physically associate with the MRN complex.

SNF2-family fork remodelers favor the association of MRE11 to stalled forks in BRCA1-deficient cells

To determine whether SMARCAL1, ZRANB3 and HLTF promote MRE11-dependent nascent DNA degradation by favoring the recruitment of MRE11 to stalled forks in BRCA1-deficient cells, we employed a proximity ligation assay (PLA)-based approach that measures the association of proteins to nascent DNA (Petruk et al., 2012). In this assay, MCF10A cells were labeled with EdU for 10 min and subsequently treated with 4 mM HU for 3 hrs (Figure 4A). Biotin was then conjugated to EdU by click chemistry and PLA was conducted to detect protein binding to biotin-labeled nascent DNA. As a control in this assay, we

performed a biotin/biotin PLA to monitor EdU-labeled replication sites (Figure 4B and S4D). To test the validity of this approach in detecting protein perturbations occurring at stalled forks, we utilized this PLA-based approach to measure the association of RPA2, γH2AX and PCNA with nascent DNA after replication stress. These studies revealed that RPA2 and γH2AX are enriched at nascent DNA after replication stress, while PCNA association is decreased under the same conditions (Figure S4B–C), as previously observed using iPOND (Dungrawala et al., 2015).

Using this PLA-based approach, we observed that HU-treated BRCA1-depleted MCF10A cells exhibited a 2-fold increase in the number of MRE11/biotin PLA foci, which occurred without significant alteration of the number of replication sites marked by biotin/biotin PLA foci, suggesting that MRE11 is increasingly associated with nascent DNA in BRCA1-deficient cells after replication stress (Figure 4B–C). Notably, depletion of SMARCAL1 or ZRANB3 led to a 2-fold reduction in the number of MRE11/biotin PLA foci induced by BRCA1 deficiency (Figure 4B–C). Similar reduction of MRE11/biotin PLA foci was also obtained when HLTF was depleted in BRCA1-deficient cells (Figure S4E), indicating that SMARCAL1, ZRANB3 and HLTF promote the association of MRE11 with nascent DNA at stalled forks in BRCA1-deficient cells. Importantly, reconstitution of SMARCAL1 KO cells with WT, but not ATPase-defective, SMARCAL1 proteins, restored the number of MRE11/biotin PLA foci in BRCA1-deficient cells, thus suggesting that MRE11 recruitment to stalled forks depends on the ATP-dependent fork-remodeling activity of SMARCAL1 (Figure 4D–E).

Reversed forks catalyzed by SMARCAL1 are degraded by MRE11 in BRCA1-deficient cells

Based on the results of the PLA and DNA fiber assays described above, we hypothesized that MRE11-mediated processing of stalled forks in BRCA1-deficient cells could depend on the formation of reversed forks catalyzed by SMARCAL1. To test this hypothesis, we monitored by electron microscopy the formation of reversed forks in HU-treated SMARCAL1- and/or BRCA1-depleted MCF10A cells with or without mirin (Figures 5A and S5A). As shown in Figure 5B, SMARCAL1 depletion led to a 2-fold reduction in the percentage of HU-induced reversed forks, confirming that SMARCAL1 plays a key role in promoting fork reversal in mammalian cells. We additionally noted that BRCA1 depletion impaired the accumulation of reversed forks upon HU treatment in a manner comparable to SMARCAL1 depletion (Figure 5B). Remarkably, mirin treatment restored the percentage of reversed forks to wild-type levels in BRCA1-deficient cells but not in BRCA1/SMARCAL1 co-depleted cells (Figure 5B). Similar results were obtained in an independent experiment, confirming the validity of our observations (Figure S5B). These observations indicate that reversed forks generated by SMARCAL1 are degraded by MRE11 in BRCA1-deficient cells.

The MRN complex degrades reversed forks generated in vitro by SMARCAL1 and ZRANB3

To test whether MRE11 could nucleolytically process reversed forks in vitro, we generated reversed fork intermediates by incubating recombinant SMARCAL1 or ZRANB3 protein with a migratable plasmid-sized replication fork structure, which we and others have previously utilized to characterize SMARCAL1 and ZRANB3 fork reversal activities

(Figures 5C and S5C) (Betous et al., 2012; Ciccia et al., 2012). Fork reversal was monitored by BamHI-mediated restriction digestion of a 5′ ^{32}P-labeled duplex DNA arm generated by the annealing of reversed DNA strands (Figure 5C). As previously shown, WT, but not helicase-dead (HD), SMARCAL1 and ZRANB3 proteins catalyzed the reversal of the plasmid-sized fork structure (Figure 5D and S5D) (Ciccia et al., 2012). Notably, addition of purified MRN or MR (MRE11-RAD50) complexes to the fork reversal reaction led to a 1.2- to 2.3-fold decrease in the ^{32}P-labeled DNA fragment generated by BamHI upon SMARCAL1- or ZRANB3-mediated fork reversal (Figure 5D, compare lanes 2 and 3; Figure 5E–F, compare lanes 2,3 and 7; Figure S5D, compare lanes 1 and 2). Interestingly, we did not observe a reduction in the ^{32}P-labeled restriction fragment when a nuclease-defective MRN complex (Anand et al., 2016) was added to the fork reversal reaction, indicating that loss of the BamHI-induced restriction fragment is dependent on MRE11 nuclease activity (Figure 5E–F, compare lanes 2, 3 and 5). The promotion of MRE11-dependent degradation of reversed forks by SMARCAL1 and ZRANB3 is not due to direct stimulation of MRE11 nuclease activity, given that SMARCAL1 and ZRANB3 did not enhance MRE11-dependent degradation of dsDNA and splayed-arm DNA structures (Figure S5E–F). Together, these observations indicate that MRE11 is able to nucleolytically process reversed forks generated by SMARCAL1 and ZRANB3.

Depletion of SNF2-family fork remodelers reduces replication stress-induced DNA damage and chromosomal instability in BRCA1/2-deficient cells

Defective maintenance of fork stability in BRCA1/2-deficient cells results in the accumulation of chromosomal aberrations in response to various agents that induce replication stress, including HU, CPT, PARP inhibitors and the DNA crosslinking agent cisplatin (Ray Chaudhuri et al., 2016; Schlacher et al., 2011; Schlacher et al., 2012). To test whether depletion of SNF2-family fork remodelers reduces replication stress-induced DNA damage in BRCA1/2-deficient cells, MCF10A cells expressing BRCA1/2 and/or SMARCAL1 shRNAs were treated with 100 nM CPT under conditions that induce SMARCAL1-dependent nascent DNA degradation (Figure S1A) and subsequently subjected to neutral comet assay to detect the formation of DSBs (Figure 6A–B). As shown in Figure 6A, depletion of SMARCAL1 with two independent shRNAs reduced the mean comet tail moment in BRCA1/2-deficient cells, suggesting that SMARCAL1 causes DNA damage in BRCA1/2-deficient cells in response to replication stress. Reduction in replication stress-induced DNA damage upon SMARCAL1 depletion in BRCA1/2-deficient cells was also observed by alkaline comet assay, which detects both single- and double-stranded DNA breaks (Figure S6A–B). In agreement with a role for SNF2-family fork remodelers in causing DNA damage in BRCA1/2-deficient cells, depletion of ZRANB3 also reduced the levels of DSBs in BRCA1/2-deficient cells in response to CPT treatment and no further reduction in DSB formation was observed when ZRANB3 and SMARCAL1 were co-depleted in BRCA1-deficient cells (Figures 6A–B and S6C–D). Similarly, depletion of HLTF was also noted to decrease the formation of DSBs in BRCA1-deficient cells (Figure S6E). Taken together, these data indicate that SNF2-family fork remodelers exacerbate replication stress-induced DNA damage in BRCA1/2-deficient cells.

To determine which activities of SMARCAL1 are required to induce DSB formation in BRCA1/2-deficient cells, SMARCAL1 KO MCF10A cells were complemented with either WT or mutant SMARCAL1 proteins. As shown in Figure 6C, WT, but not R764Q- or $\Delta N_{1\text{-}115}$-mutant, SMARCAL1 caused DSB formation in BRCA1-deficient cells upon CPT treatment, indicating that that the ATP-dependent fork-remodeling and RPA-binding activities of SMARCAL1 are required to induce DSBs in BRCA1-deficient cells. Similar experiments conducted in BRCA1/ZRANB3 co-depleted cells revealed that DNA break formation was restored by expression of WT ZRANB3, but not ZRANB3 mutants defective in ATP-dependent fork remodeling (K163D), association with PCNA (PIP+APIM) or binding to its polyubiquitinated form ($NZF_{\text{-zinc}}$) (Figure 6D), indicating that replication stress-induced DNA breaks in BRCA1-deficient cells depend on ZRANB3 fork-remodeling activity and on its association with polyubiquitinated PCNA.

To determine the impact of SMARCAL1 or ZRANB3 depletion on replication stress-induced chromosomal instability in BRCA1/2-deficient cells, MCF10A cells depleted of BRCA1/2 and/or SMARCAL1 (or ZRANB3) were treated with 100 nM CPT for 5 hrs and the number of CPT-induced chromosomal aberrations was determined following imaging of metaphase spreads. As previously reported (Ray Chaudhuri et al., 2016; Schlacher et al., 2011; Schlacher et al., 2012), BRCA1/2 deficiency led to an increased number of replication stress-induced chromosomal aberrations (Figure 6E–F). Interestingly, depletion of SMARCAL1 or ZRANB3 reduced the formation of chromosomal abnormalities in BRCA1/2-deficient cells upon CPT treatment (Figure 6E–F). Similar findings were obtained by depleting SMARCAL1 or ZRANB3 with a second shRNA in CPT-treated BRCA1-deficient cells (Figure S6F). Altogether, these studies indicate that SNF2-family fork remodelers cause chromosomal instability in BRCA1/2-deficient cells in response to replication stress.

SMARCAL1 depletion promotes chemoresistance in BRCA1-deficient breast cancer cells

Previous studies have reported that low expression of PTIP, a DNA repair factor whose deficiency causes restoration of fork stability and chemoresistance in BRCA1/2-deficient cancer cells, is associated with poor prognosis in patients with BRCA1/2-mutant ovarian cancer (Ray Chaudhuri et al., 2016). Our observation that low SMARCAL1 expression is associated with poor survival outcome in patients with invasive BRCA1-mutant breast cancer (Figures S7A) raised the possibility that SMARCAL1 expression could influence the response of BRCA1-mutant breast tumors to chemotherapeutic treatments. To test this hypothesis, we conducted cell survival assays in invasive ductal breast cancer MDA-MB-231 cells subjected to RNAi-mediated depletion of BRCA1 and/or SMARCAL1 (Figure 7A) and treated with the DNA crosslinking agent cisplatin, the PARP inhibitor olaparib or CPT. Notably, SMARCAL1/BRCA1 co-depleted MDA-MB-231 cells exhibited a mild but significant increase in resistance to cisplatin, olaparib and CPT compared to BRCA1-deficient cells (Figures 7B and S7B). In agreement with these findings, SMARCAL1 depletion increased the resistance of BRCA1-mutant breast cancer MDA-MB-436 cells to cisplatin, olaparib and CPT (Figures 7C and S7C–D). SMARCAL1 depletion, however, did not confer chemoresistance to BRCA1-deficient mammary epithelial MCF10A cells (Figure S7E), potentially underlying cell-type specific mechanisms by which fork protection

contributes to chemoresistance, as discussed below. Chemoresistance in BRCA1-deficient MDA-MB-231 cells was accompanied by re-establishment of fork stability, without restoration of HDR, as detected by DNA fiber and RAD51 foci formation assays (Figures 7D and S7F). These findings are consistent with previous studies suggesting that restoration of fork stability promotes chemoresistance in BRCA1/2-deficient cells in an HDR-independent manner (Ray Chaudhuri et al., 2016).

DISCUSSION

Fork remodeling is required for nascent DNA degradation in BRCA1/2-deficient cells

In this study we report that the degradation of nascent DNA observed in BRCA1/2-deficient cells upon replication stress is dependent on fork remodelers of the SNF2 family. We have previously shown that the DNA translocase SMARCAL1 is recruited by the RPA complex to stalled forks and catalyzes the ATP-dependent reversal of replication fork structures in vitro (Ciccia et al., 2009; Ciccia et al., 2012). Here we utilize electron microscopy to show that SMARCAL1 is required for efficient formation of reversed forks in mammary epithelial cells, indicating that SMARCAL1 plays a key role in the remodeling of stalled forks in vivo (Figure 5B). Our observation that SMARCAL1 mutants defective in RPA-mediated recruitment to stalled forks and ATP-dependent fork remodeling are unable to promote nascent DNA degradation in BRCA1/2-deficient cells (Figure 1G) indicates that the fork instability of BRCA1/2-deficient cells is dependent on the remodeling of stalled forks by SMARCAL1. In agreement with these findings, SMARCAL1-mediated fork remodeling promotes replication stress-induced degradation of nascent DNA in *X. laevis* egg extracts depleted of BRCA2 (Kolinjivadi et al., 2017).

BRCA1/2 and RAD51 protect reversed forks from MRE11-dependent degradation

Our studies indicate that SMARCAL1 utilizes its fork-remodeling activity to promote MRE11 recruitment to nascent DNA at stalled forks in BRCA1-deficient cells (Figure 4E). On the basis of this observation and our electron microscopy studies (Figure 5B), we propose that SMARCAL1 induces MRE11-dependent degradation of nascent DNA in BRCA1/2-deficient cells by catalyzing the formation of reversed forks. Under those circumstances, MRE11 can nucleolytically process the extruded arm of reversed forks, as shown by our biochemical assays (Figure 5D–F). Our finding that reversed forks are degraded by MRE11 in BRCA1/2-deficient cells (Figure 5B) reveals that BRCA1/2 protect reversed forks, possibly by loading RAD51 onto ssDNA tails generated upon fork reversal (Kolinjivadi et al., 2017). In support of this notion, RAD51 overexpression prevents fork instability in BRCA2-deficient cells (Schlacher et al., 2011) and WT, but not DNA-binding mutant ($RAD51^{T131P}$), forms of RAD51 stably associate with reversed fork structures and protect them from MRE11-dependent degradation (Kolinjivadi et al., 2017). In agreement with these findings, we show that inhibition of RAD51 DNA-binding activity by the small molecule B02 causes SMARCAL1-dependent nascent DNA degradation (Figure 1E). These data indicate that RAD51 inhibition by B02 destabilizes reversed forks, thus mimicking the effects induced by the $RAD51^{T131P}$ mutation, without causing the defects in fork reversal previously observed upon RAD51 depletion (Zellweger et al., 2015).

Besides restoring fork stability in cells with BRCA1/2 or RAD51 deficiency, SMARCAL1 depletion also prevents HU-induced nascent DNA degradation caused by FANCD2 deficiency (Figure 1D), suggesting that the FA pathway may cooperate with BRCA1/2 in protecting reversed forks, possibly by stabilizing RAD51-DNA complexes (Sato et al., 2016; Schlacher et al., 2012). RAD51 defects resulting from the $RAD51^{T131P}$ mutation have indeed been identified in an FA patient (Wang et al., 2015). Based on these observations, we predict that the nascent DNA degradation caused by inactivation of other factors that stabilize RAD51-DNA complexes, such as BOD1L and WRNIP1 (Higgs et al., 2015; Leuzzi et al., 2016), might also depend on SMARCAL1-mediated fork reversal.

Nascent DNA degradation in BRCA1/2-deficient cells depends on a multitude of SNF2-family fork remodelers

The requirement for fork reversal in mediating nascent DNA degradation is further supported by our findings that the degradation of nascent DNA can also be inhibited in BRCA1/2-deficient cells by depleting other DNA translocases that remodel replication forks, such as ZRANB3 and HLTF (Figure 3B–D). Similar to SMARCAL1, ZRANB3 is also required for the formation of reversed forks in mammalian cells (Vujanovic et al., 2017) and ZRANB3-mediated fork reversal promotes MRE11-dependent degradation of reversed fork structures in vitro (Figure 5E). Moreover, ZRANB3 and HLTF, like SMARCAL1, promote the association of MRE11 to nascent DNA at stalled forks in BRCA1-deficient cells (Figures 4C and S4E). Interestingly, depletion of either SMARCAL1, ZRANB3 or HLTF alone is sufficient to entirely abrogate nascent DNA degradation in BRCA1/2-deficient cells (Figures 1C and 3B–D), raising the possibility that the above fork remodelers may co-operate to promote the degradation of stalled forks in BRCA1/2-deficient cells. Biochemical studies have shown that SMARCAL1, ZRANB3 and HLTF recognize distinct types of stalled fork structures (Betous et al., 2013; Betous et al., 2012; Hishiki et al., 2015; Kile et al., 2015). In particular, SMARCAL1 preferentially remodels fork structures with a ssDNA gap on the leading-strand, while ZRANB3 reverses equally efficiently fork intermediates with either leading- or lagging-strand gaps and HLTF acts upon fork structures that expose a 3′-hydroxyl group on the blocked leading-strand (Betous et al., 2013; Betous et al., 2012; Hishiki et al., 2015; Kile et al., 2015). We propose that the extensive resection observed in BRCA1/2-deficient cells upon HU treatment (~10 kbp in 5 hrs) (Schlacher et al., 2011; Schlacher et al., 2012) occurs through multiple rounds of fork reversal, resection, and restoration, during which different stalled fork structures might be generated. As such, this process would require several fork-remodeling enzymes with distinct substrate specificities, such as SMARCAL1, ZRANB3 and HLTF. Our studies have indeed revealed that the fork-remodeling activities of all the above factors are necessary for nascent DNA degradation in BRCA1-deficient cells (Figures 1G and 3E–F). Besides promoting fork reversal under the above circumstances, fork remodelers may also mediate fork restoration prior to a subsequent round of fork reversal and resection. Previous studies have indeed shown that SMARCAL1 and ZRANB3 possess fork restoration activities (Betous et al., 2013). HLTF could promote the above processes also by mediating PCNA polyubiquitination and consequently favoring ZRANB3-dependent nascent DNA degradation in BRCA1/2-deficient cells. The association of ZRANB3 with polyubiquitinated PCNA is in fact required for fork

reversal (Vujanovic et al., 2017) and for mediating nascent DNA degradation in BRCA1-deficient cells (Figure 3E).

Besides SMARCAL1, ZRANB3 and HLTF, other DNA helicases/translocases have been shown to remodel stalled forks, including FANCM, FBH1, RECQL5 and RAD54 (Neelsen and Lopes, 2015). We have shown that RECQL5 is not required to promote nascent DNA degradation in BRCA1-deficient cells (Figure S3C–D). In agreement with these findings, previous studies have shown that RECQL5 depletion does not prevent fork degradation occurring upon RAD51 destabilization induced by BOD1L depletion (Higgs et al., 2015). Future studies will be required to determine whether other fork remodelers also promote nascent DNA degradation in BRCA1/2-deficient cells and define how they might cooperate to cause fork instability in those cells.

SNF2-family fork remodelers promote genomic instability in BRCA1/2-deficient cells

Our studies show that the re-establishment of fork stability in BRCA1/2-deficient cells by depletion of SMARCAL1, ZRANB3 or HLTF is accompanied by a marked reduction of replication stress-induced DNA damage and genomic instability (Figures 6A and S6E). These findings are in agreement with previous observations that the chromosomal instability of BRCA1/2-deficient cells can be reduced by inhibiting the nuclease activity of MRE11 or by preventing the recruitment of MRE11 to stalled forks by PARP1, CHD4, MLL3/4 and PTIP (Ding et al., 2016; Guillemette et al., 2015; Ray Chaudhuri et al., 2016; Schlacher et al., 2011; Schlacher et al., 2012). Our observations that WT, but not fork remodeling-defective, SMARCAL1 and ZRANB3 proteins cause replication stress-induced DSBs in BRCA1-deficient cells (Figure 6C–D) indicate that the remodeling of stalled forks by SMARCAL1 and ZRANB3 causes genomic instability in BRCA1-deficient cells. According to our electron microscopy studies on replication intermediates, SMARCAL1 and MRE11 promote the formation of large ssDNA gaps (> 300 nts) at stalled forks in BRCA1-deficient cells (Figure 2B). These observations suggest that the degradation of reversed forks leads to formation of large ssDNA gaps in BRCA1-deficient cells, which might in turn generate mitotic ultrafine bridges and thereby cause chromosomal instability, as recently suggested by studies in yeast (Ait Saada et al., 2017). In addition, the formation of reversed forks might induce fork cleavage by the MUS81 and SLX4 nucleases, thus generating DSBs that could be aberrantly repaired in BRCA1/2-deficient cells (Ciccia and Symington, 2016). Taken together, our observations underscore the importance of replication fork stability in suppressing genomic aberrations induced by replication stress.

Replication fork protection in cancer predisposition and chemoresistance

The precise mechanisms by which BRCA1/2 suppress breast and ovarian cancer remain poorly understood. Recent studies have reported that the mammary epithelial cells of BRCA1 mutation carriers exhibit defective protection of stalled replication forks despite being fully functional for other BRCA1 activities, including DSB repair by HDR and DNA damage checkpoint signaling (Pathania et al., 2014). Extensive replication stress-induced fork degradation was also recently observed in cells carrying BRCA2 heterozygous truncating mutations (Tan et al., 2017). These observations raise the possibility that maintenance of replication fork stability is a key early event in BRCA1/2-mediated tumor

suppression. Future work will be necessary to determine whether tumor suppression can be restored to BRCA1/2-mutant cells by re-establishing fork protection upon inhibition of SMARCAL1, ZRANB3 or HLTF.

While inhibition of fork remodelers might be considered as a means to suppress BRCA1/2-mutant tumor formation prophylactically, it may also act, similarly to CHD4 or PTIP inactivation (Guillemette et al., 2015; Ray Chaudhuri et al., 2016), to render pre-existing BRCA1/2-deficient tumors resistant to replication stress-inducing chemotherapeutic agents, thus accelerating tumor progression. Indeed, our studies revealed that SMARCAL1 depletion rendered BRCA1-deficient breast cancer cells resistant to replication stress-inducing agents (Figure 7). Interestingly, chemoresistance was not observed when SMARCAL1 was depleted in BRCA1-deficient non-malignant mammary epithelial cells, despite the restoration of genomic stability induced in those cells by SMARCAL1 depletion (Figures 6 and S7E). The distinct response to SMARCAL1 depletion in these cell lines may reflect cell-type specific mechanisms by which fork protection could contribute to chemoresistance. In line with this hypothesis, lack of fork protection is accompanied by sensitivity to replication stress-inducing agents in BRCA1/2-deficient B lymphocytes, U2OS cells and ovarian cancer cells (Ding et al., 2016; Dungrawala et al., 2017; Ray Chaudhuri et al., 2016), while it does not result in significant alterations of cell viability in BRCA2-deficient hamster cells, HeLa cells and human breast epithelial cells subjected to replication stress (Schlacher et al., 2011; Tan et al., 2017). Future studies will be required to unravel the pathways by which fork protection may elicit chemoresistance.

On the basis of the above considerations, it would therefore be important to determine whether restoration of fork protection in BRCA1/2-mutant cells could have both anti- and pro-tumorigenic properties. These studies could have important implications for the development of therapeutic opportunities for preventing and/or treating BRCA1/2-mutant tumors.

STAR METHODS

CONTACT FOR REAGENT AND RESOURCE SHARING

Further information and requests for resources and reagents should be directed to and will be fulfilled by the Lead Contact, Alberto Ciccia (ac3685@cumc.columbia.edu).

EXPERIMENTAL MODEL AND SUBJECT DETAILS

Cell lines—MCF10A cells were maintained in a 1:1 mixture of DMEM and Ham's F12 medium (Thermo Fisher Scientific), supplemented with 5% horse serum (Thermo Fisher Scientific), 20 ng/ml human epidermal growth factor (Peprotech), 100 ng/ml cholera toxin, 10 μg/ml insulin and 0.5 μg/ml hydrocortisone (Sigma-Aldrich). hTERT-immortalized SD31 fibroblasts (Ciccia et al., 2009) and PD20 cells (Sims et al., 2007) were maintained in DMEM medium (Thermo Fisher Scientific) containing 15% Fetalgro bovine growth serum (RMBIO). The human embryonic kidney fibroblast cell line HEK293T was maintained in DMEM supplemented with 10% Fetalgro bovine growth serum. MDA-MB-231 and MDA-MB-436 cell lines were maintained in DMEM supplemented with 10% Fetalgro bovine

growth serum. The MCF10A, MDA-MB-231 and MDA-MB-436 cell lines used in this study have been authenticated by short tandem repeat DNA profiling (Genetic Resources Core Facility at Johns Hopkins University).

METHOD DETAILS

DNA clones—pDONR223-SMARCAL1, pDONR223-SMARCAL1-R586W and pDONR223-SMARCAL1-R764Q constructs have been previously described (Ciccia et al., 2009). pDONR223-SMARCAL1-$\Delta N_{1\text{-}115}$ was generated by PCR-amplification of pDONR223-SMARCAL1 (Ciccia et al., 2009) using the DNA oligos SL1-$\Delta N_{1\text{-}115}$-FW and SL1-$\Delta N_{1\text{-}115}$-RV. siRNA resistant pDONR201-ZRANB3 and pDONR201-ZRANB3-PIP +APIM constructs have been previously described (Ciccia et al., 2012). siRNA-resistant pDONR201-ZRANB3-K163D was generated by introducing the K163D mutation into siRNA-resistant pDONR201-ZRANB3 by inverse PCR using the DNA oligos ZR3-K163-FW and ZR3-K163-RV. siRNA-resistant pDONR201-ZRANB3-$NZF_{\text{-zinc}}$ was generated by introducing the C641A and C644A mutations into siRNA-resistant pDONR201-ZRANB3 using the DNA oligos ZR3-NZF-FW and ZR3-NZF-RV. pDONR223-HLTF was obtained from the Orfeome v8.1 library (ID #100070304). siRNA-resistant mutations in pDONR223-HLTF were introduced by inverse PCR using the DNA oligos HLTFsiRes-FW and HLTFsiRes-RV. siRNA-resistant pDONR223-HLTF-HIRAN was obtained by introducing the R71E mutation into siRNA-resistant pDONR223-HLTF using the DNA oligos HLTF-HIRAN-FW and HLTF-HIRAN-RV. STOP codons were introduced into pDONR223-SMARCAL1, pDONR223-HLTF and pDONR201-ZRANB3 prior to Gateway LR recombination (Thermo Fisher Scientific) into the lentiviral expression vector pHAGE-C-FLAG-HA-DEST (Guarani et al., 2014) and the retroviral expression vector pMSCV-N-HA-FLAG (Ciccia et al., 2009). DNA oligo sequences are available in Table S1.

Recombinant viral production and infection—Recombinant retroviruses and lentiviruses were generated by co-transfecting helper packaging vectors together with retroviral or lentiviral vectors into HEK293T cells using the *Trans*IT-293 transfection reagent (Mirus). Virus-containing supernatants were collected 48 hrs after transfection and utilized to infect MCF10A and HEK293T cells in the presence of 8 μg/ml polybrene. 48 hrs after viral addition, MCF10A and HEK293T cells were selected using 1 μg/ml puromycin or 10 μg/ml blasticidin for 3–5 days.

RNAi treatment—The following retroviral vectors have been used to express shRNAs in this study: pMSCV-PURO and pMSCV-BLAST vectors containing control firefly luciferase shRNA, BRCA1 shRNA, BRCA2 shRNA, SMARCAL1 shRNA #1, SMARCAL1 shRNA #2, ZRANB3 shRNA #1, ZRANB3 shRNA #2 (Key Resources Table). Combinatorial stable shRNA-mediated knockdown of control, BRCA1/2, SMARCAL1 and/or ZRANB3 in MCF10A cells was achieved by two sequential rounds of infection and selection using recombinant viral particles derived from the above retroviral vectors carrying resistance to puromycin or blasticidin. SMARCAL1-deficient SD31 fibroblasts complemented with WT and R586W-mutant SMARCAL1 (Ciccia et al., 2009) and SMARCAL1 KO cells complemented with WT, R764Q- and $\Delta N_{1\text{-}115}$-mutant SMARCAL1 were transfected with control or BRCA1 siRNA (GE Dharmacon; Table S1) using lipofectamine RNAiMAX

(Thermo Fisher Scientific) according to manufacturer's instructions and subjected to DNA fiber and genomic stability assays 3 days after transfection. Complementation studies in ZRANB3- and HLTF-deficient cells were conducted as follows: MCF10A cells were transduced with viral particles generated from lentiviral pHAGE constructs encoding for siRNA-resistant WT, PIP+APIM-, NZF_{-zinc}- or K163D-mutant ZRANB3, WT or HIRAN-mutant HLTF and subsequently selected with puromycin to stably express exogenous siRNA-resistant WT and mutant proteins. Cells expressing siRNA-resistant WT and mutant ZRANB3 or HLTF proteins were transfected with siRNAs targeting firefly luciferase (control siRNA, GE Dharmacon), ZRANB3 (GE Dharmacon), HLTF (Thermo Fisher Scientific) and/or BRCA1 (GE Dharmacon) using lipofectamine RNAiMAX and subjected to DNA fiber and DNA damage assays 3 days after transfection. SMARCAL1 siRNA #3 (GE Dharmacon) was used to deplete SMARCAL1 in PD20 cells for DNA fiber analysis. SMARCAL1 siRNA #1 (GE Dharmacon), siRNA #2 (GE Dharmacon), siRNA #3 (GE Dharmacon) and BRCA1 siRNA (GE Dharmacon) were utilized to deplete SMARCAL1 and BRCA1 in MDA-MB-231 and MDA-MB-436 cells subjected to survival assays. HLTF (Thermo Fisher Scientific) and RECQL5 (GE Dharmacon) siRNAs were utilized to deplete HLTF and RECQL5 in control and BRCA1/2-depleted MCF10A cells. The siRNA sequences are available in Table S1.

Generation of SMARCAL1 knock-out cells—SMARCAL1 knock-out (KO) MCF10A cells were obtained by CRISPR-Cas9 technology using an eCas9-P2A-Puro plasmid. This construct was generated by initially amplifying the puromycin resistance gene from pHAGE-C-HA-FLAG-DEST (Guarani et al., 2014) with oligonucleotides containing the P2A sequence. The purified PCR product was then fused to EcoRI-digested eSpCas9 (1.1) (Addgene plasmid #71814) by Gibson assembly. Guide RNAs targeting *SMARCAL1* were designed with the online tool at crispr.mit.edu, synthesized (Integrated DNA Technologies) and ligated into BbsI-digested eCas9-P2A-Puro. The two gRNAs target exon 3 of *SMARCAL1* (Key Resources Table). MCF10A cells were transfected with *SMARCAL1* gRNA-containing eCas9-P2A-Puro plasmids using Lipofectamine 3000 (Thermo Fisher Scientific) and briefly selected with puromycin (1 μg/ml) for 48 hrs. Transfected cells were then re-plated at low density without puromycin selection for colony formation. Colonies were subsequently isolated and screened by western blotting for loss of SMARCAL1 expression. Genetic modification of exon 3 of *SMARCAL1* in KO clone #31 was verified by Sanger sequencing of amplicons from genomic DNA. SMARCAL1 KO cells were then transduced with viral particles generated from lentiviral pHAGE constructs encoding for WT, R764Q- and ΔN_{1-115}-mutant SMARCAL1 and subsequently selected with puromycin to stably express the exogenous WT and mutant proteins.

Single-molecule analysis of DNA replication—Exponentially growing MCF10A cells were pulse-labeled with 25 μM CldU (15 min), washed and exposed to 125 μM IdU (25 min). PD20 cells were pulse-labeled with 25 μM CldU (20 min), washed and exposed to 125 μM IdU (20 min). SD31 cells (Ciccia et al., 2009) were pulse-labeled with 250 μM IdU (15 min), washed and exposed to 100 μM CldU (40 min). After exposure to the second nucleotide analog, the cells were washed again in warm 1X PBS and treated or not for 5 hrs with hydroxyurea (HU, 2 mM, Sigma-Aldrich), HU + mirin (50 μM, Sigma-Aldrich), HU +

RAD51 inhibitor (B02) (25 μM, Calbiochem) or camptothecin (CPT, 100 nM, Sigma-Aldrich). Labeled cells were trypsinized and resuspended in ice-cold PBS at 4×10^5 cells/ml. Two microliters of this suspension were spotted onto a pre-cleaned glass slide and lysed with 10 μl of spreading buffer (0.5% SDS in 200 mM Tris-HCl, pH 7.4 and 50 mM EDTA). After 6 min, the slides were tilted at 15° relative to hori zontal, allowing the DNA to spread. Slides were air-dried, fixed in methanol and acetic acid (3:1) for 2 min, rehydrated in PBS for 10 min and denatured with 2.5 M HCl for 50 min at room temperature. Slides were then rinsed in PBS and blocked in PBS + 0.1% Triton X-100 (PBS-T) + 5% BSA for 1 hr at room temperature. Rat anti-BrdU (1:100, AbD Serotec, MCA2060T) and mouse anti-BrdU (1:100, Becton Dickinson, 347580) were then applied to detect CldU and IdU, respectively. After a 1 hr incubation, slides were washed in PBS and stained with Alexa Fluor 488-labelled goat anti-mouse IgG1 antibody and Alexa Fluor 594-labelled goat anti-rat antibody (1:300 each, Thermo Fisher Scientific). Slides were mounted in Prolong Gold Antifade (Thermo Fisher Scientific) and held at −20°C. Replication tracks were imaged on a Nikon Eclipse 50i microscope fitted with a PL Apo 40X/0.95 NA objective and measured using ImageJ software. In each experiment, 200 or more individual tracks were measured for fork degradation estimation. Data are representative of at least 2 independent experiments.

Electron microscopy—DNA analysis by electron microscopy was performed as previously described (Neelsen et al., 2014) with some modifications. Briefly, for each sample $2.5–5.0 \times 10^7$ cells were collected. After standard trypsinization cells were transferred to 50 ml Falcon tubes and spun down at 600 g for 5 min. The cell pellet was washed once with 5 ml of ice-cold 1X PBS, resuspended in 10 ml ice-cold 1X PBS and transferred to 60 × 15 mm tissue culture plate, to which 10 μg/ml TMP (Trimethylpsoralen, T6137 Sigma-Aldrich) were added. The petri dish was incubated in the dark for 5 min on a pre-cooled metal surface and then UV-irradiated for 5 min in a Stratalinker equipped with monochromatic 365 nm lamps. The cycle of TMP addition, dark incubation and irradiation was repeated four times. Cells were then transferred to a 15 ml tube, washed twice with 1 ml PBS and DNA was extracted using QIAGEN genomic DNA extract kit according to manufacturer instructions. The DNA pellet was resuspended in standard TE buffer. 30 μgs of genomic DNA were digested with 150 U of PvuII HF restriction enzyme (New England Biolabs) for 3.5 hrs at 37°C. DNA replication intermediates were further enriched in the final DNA sample by using 1 ml (slurry) of BND-cellulose resin (Sigma-Aldrich, B6385) as previously described (Neelsen et al., 2014). DNA was finally cleaned using Amicon Ultra-0.5 Centrifugal Filter Unit with Ultracel-100 (Millipore, UFC510096). DNA samples were loaded on a 0.8% agarose gel to check for DNA quality and concentration. The DNA was then processed for rotary shadowing and platinum coating as previously shown (Neelsen et al., 2014) using a Med20 evaporator (Leica). Images were acquired at the IFOM EM facility using TECNAI12 electron microscope equipped with a GATAN camera run by Digital Micrograph software. Data are representative of 2 independent experiments.

Comet assay—Single- and double-stranded DNA breaks were evaluated by alkaline comet assay and neutral comet assay (single-cell gel electrophoresis). MCF10A cells were plated in 12-multiwell plates (100,000 cells/well) and the following day treated or not with HU (2 mM, Sigma-Aldrich) or CPT (100 nM, Sigma-Aldrich) for 5 hrs before collection.

The cells collected were then mixed with molten LMAgarose and pipetted onto CometSlide (double layer of 1% of NMAgarose). In the neutral comet assay, the slides were incubated with a lysis solution (30 mM EDTA, 0.5% SDS) for 1 hr, and then placed in horizontal chambers (FisherBiotech) to perform electrophoresis at 20 V for 20 min in TBE. After washing with water, and fixing with ice-cold ethanol for 5 min, the slides were stained with a fluorescent dye (GelRed, Biotium, 1:1,000 in water). In the alkaline comet assay, the slides were incubated with a lysis solution at pH 10 (25 mM NaCl, 100 mM EDTA, 10 mM Tris base) for 16 hrs and with an alkaline solution at pH 13 (300 mM NaOH, 1 mM EDTA) for 20 min. The slides were then placed in horizontal chambers (FisherBiotech) and alkaline electrophoresis was performed at 25 V for 20 min. After incubation with a neutralization buffer (0.4 M Tris-HCl, pH 7.5) for 15 min, followed by ice-cold ethanol for 5 min, the slides were stained with ethidium bromide (20 μg/ml, Sigma-Aldrich). In both assays, at least 75 cells were analyzed for each experimental point using a Nikon Eclipse 50i microscope. To assess the amount of DNA damage, comet tail moment values were determined using CometScore Software Version 1.5. Apoptotic cells (small comet head and very large comet tail) were excluded from the analysis. Data are representative of 2 independent experiments.

Chromosome spreads—MCF10A cells were treated with CPT (100 nM, Sigma-Aldrich) for 5 hrs. Cells were washed in PBS and recovered in fresh media for 24 hrs before colcemid arrest (0.2 μg/ml for 5 hrs). Cells were harvested by trypsinization, incubated in 75 mM KCl for 20 min at 37°C and fixed in a methanol/acetic acid (3: 1) solution. The fixed suspension was dropped onto slides to obtain chromosome spreads that were stained with Giemsa (Sigma-Aldrich) and visualized using a BX61TRF Olympus microscope connected to an automated Leica GSL scanner. Metaphase spreads were captured with an APO 100X, 0.7 NA oil immersion objective. For each condition 25 metaphases or more were examined blindly by 2 independent investigators. Data are representative of 2 independent experiments.

Survival Assay—Cells were seeded into 24-well plates at a density of 5×10^3 cells per well (MDA-MB-231 cells) or 2.5×10^3 cells per well (MCF10A cells) and treated with cisplatin (Sigma-Aldrich), CPT (Sigma-Aldrich), or olaparib (AZD2281, SelleckChem) at the indicated concentrations. After incubation for 5 to 7 days, cell survival was assessed by crystal violet staining. Adherent cells were fixed and stained with a solution containing 1% formaldehyde and 1% crystal violet in methanol. The absorbed dye was resolubilized with methanol containing 0.1% SDS, which was then transferred into 96-well plates and measured photometrically (595 nm) in a microplate reader. Cell survival was calculated by normalizing the absorbance of the treated samples to the absorbance of untreated controls. Survival curves were generated using the nonlinear regression algorithm of GraphPad Prism software (Version 6.0). Data are representative of 2 independent experiments.

Immunofluorescence—MCF10A and MDA-MB-231 cells were plated on glass coverslips in 24-multiwell plates (1×10^5 cells/well) and treated the following day with 5 Gy ionizing radiation using a JL Shepherd Mark I cesium irradiator (JL Shepherd & Associates) or incubated with 50 nM CPT. 6 hrs after irradiation or 24 hrs after incubation

with CPT, cells were fixed with 4% paraformaldehyde/PBS for 10 min, washed with PBS and permeabilized using 0.5% Triton X-100/PBS for 10 min at room temperature. Cells were subsequently incubated with a blocking solution (3% BSA/PBS) for 1 hr at room temperature and then with anti-RAD51 antibody (1:10,000, CosmoBio, BAM-70-001-EX) for 1 hr at room temperature or overnight at 4°C. RAD51 foci were detected using an Alexa Fluor 488-labelled goat anti-rabbit IgG antibody (1:1,000, Thermo Fisher Scientific). DAPI (Sigma-Aldrich) was used to stain nuclei. Images were acquired using a Nikon Eclipse 50i microscope equipped with a 40X Plan Apo λ objective and 0.95 numerical aperture (NA). The ImageJ software was used for processing images and quantifying the percentage of RAD51 foci positive cells (>5 foci for IR, >10 foci for CPT). Foci were counted in 100 or more cells per experimental condition. Each experiment was repeated 2 times independently.

Proximity ligation assay on nascent DNA—MCF10A cells were seeded on round coverslips at a density of 7.5×10^4, pulse-labeled with 10 μM EdU for 10 min followed by 4 mM HU for 3 hrs. After the indicated treatment, cells were permeabilized with 0.5% Triton for 10 min 4°C, washed with PBS, fixed at room temperature with 3% formaldehyde/2% sucrose in PBS for 10 min, washed in PBS and then blocked in 3% BSA/PBS for 30 min. After blocking, cells were subjected to Click-iT reaction with biotin-azide for 30 min and incubated overnight with the two relevant primary antibodies at 4°C. The primary antibodies were diluted in PBS with 1% BSA and 0.1% saponin (Sigma-Aldrich). The primary antibodies used were: mouse monoclonal anti-MRE11 (GeneTex, 1:100), rabbit polyclonal anti-biotin (Bethyl, 1:3000), mouse monoclonal anti-biotin (Jackson Immnunoresearch, 1:2000), mouse monoclonal anti-PCNA (Thermo Fisher Scientific, 1:1000), mouse monoclonal anti-RPA2 (Thermo Fisher Scientific, 1:1000) and mouse monoclonal anti-γH2AX (BioLegend, 1:5000). The negative control consisted of using only one primary antibody. The PLA reactions (Duolink, Sigma-Aldrich) to detect anti-biotin antibody and other antibodies used were performed according to manufacturer instructions. Images were acquired using a Nikon Eclipse 50i microscope fitted with a PL Apo 40X/0.95 NA objective and measured using Cell Profiler 2.2.0 (Broad Institute) software. Data are representative of 2 independent experiments.

Quantitative real-time PCR—Total RNA was isolated from SD31 and MCF10A cells using RNeasy kit (Qiagen). Reverse transcription was carried out with 0.5 μg of total RNA using random hexamer primers and the SuperScript III reverse transcriptase kit (Thermo Fisher Scientific). Equal amounts of cDNA were mixed with the Power SYBR green PCR master mix (Thermo Fisher Scientific) and run on a Stratagene MX3005 Real-Time PCR System. The primers used were: BRCA1-qPCR-FW and BRCA1-qPCR-RV, RECQL5-qPCR-FW and RECQL5-qPCR-RV (Table S1). BRCA1 and RECQL5 mRNA levels were determined by comparing threshold cycle values for each experimental condition relative to TBP mRNA levels.

Protein purification—MRN and MR were prepared as described before (Anand et al., 2016). Both FLAG-SMARCAL1 (wild-type or helicase-dead) and FLAG-ZRANB3 (wild-type or helicase-dead) were purified from *Sf*9 insect cells (Ciccia et al., 2012). 800 ml of cells were infected with respective baculovirus stocks, collected after 52 hrs, washed with

PBS and stored at −80°C until purification. Pellets were thawed on ice in lysis buffer (50 mM Tris-HCl, pH 7.5, 1 mM EDTA, 1:400 (v/v) protease inhibitor cocktail (Sigma-Aldrich, P8340), 30 µg/ml leupeptine, 1 mM phenylmethylsulfonyl fluoride, 0.5 mM beta-mercaptoethanol and 0.1% NP40) for 15 min, followed by the addition of NaCl (325 mM final concentration) and glycerol (16% final concentration) and incubated for 30 min. The lysate was spun at 57,000 g for 30 min at 4°C to obtain soluble extract. Soluble extract was then bound to 0.8 ml of anti-FLAG M2 affinity gel (Sigma-Aldrich, A2220) for 1 hr, washed extensively with FLAG wash buffer (lysis buffer with 1 M NaCl, followed by lysis buffer with 100 mM NaCl) and eluted with wash buffer containing 3 x FLAG peptide (100 ng/µl, Sigma-Aldrich, F4799). ZRANB3 purification included an additional step of binding to CM sepharose resin (Sigma-Aldrich) for 1 hr followed by washing with CM sepharose wash buffer (50 mM Tris-HCl, pH 7.5, 1 mM phenylmethylsulfonyl fluoride, 10% glycerol, 5 mM beta-mercaptoethanol, 100 mM NaCl) and elution with CM sepharose wash buffer with 1 M NaCl. The eluted protein was dialyzed with dialysis buffer (50 mM Tris-HCl, pH 7.5, 0.5 mM phenylmethylsulfonyl fluoride, 10% glycerol, 5 mM beta-mercaptoethanol, 100 mM NaCl). The purified proteins were aliquoted, snap frozen and stored at −80°C until use.

DNA degradation assays—The plasmid-sized replication fork (pRF) substrate was prepared as described previously (Blastyak et al., 2010). The reactions were carried out in a 10 µl volume in a reaction buffer containing 25 mM Tris-HCl (pH 7.5), 5 mM magnesium acetate, 1 mM dithiothreitol, 0.25 mg/ml BSA (New England Biolabs), 1 mM phosphoenolpyruvate, 80 U/ml pyruvate kinase, 1 mM ATP and 1 nM (in molecules) plasmid replication fork substrate. Recombinant SMARCAL1 (wild-type or helicase-dead) or ZRANB3 (wild-type or helicase-dead) proteins (50 nM each) were added and incubated for 5 min at 37°C to perform branch migration. Next, manganese acetate (5 mM final concentration) was added just before adding recombinant MRN (50 nM) or MR (50 nM) to the reaction and further incubated for 2 hrs at 37°C. The reaction products were then digested with BamHI (New England Biolabs). The reactions were stopped by adding 1 µl of Proteinase K (19 mg/ml, Roche) and 5 µl of STOP buffer (150 mM EDTA, 2% SDS, 30% glycerol, 0.25 % Bromophenol blue) for 10 min at 37°C. The products were separated on an 8% native polyacrylamide gel in TBE buffer. Gels were dried on DE81 chromatography paper (Whatman), exposed to Storage Phosphor screens and analyzed on Typhoon FLA 9500 (GE Healthcare). Degradation of BamHI fragment was quantified using Image Quant software. MR degradation assays on dsDNA and splayed arm substrates were conducted as previously described (Anand et al., 2016). Briefly, DNA substrates (5 nM) were simultaneously incubated with MR (50 nM) and SMARCAL1 or ZRANB3 proteins (25 or 50 nM) for 2 hrs at 37°C. The dsDNA substrate was prepared by annealing oligonucleotides X12-3* and X12-4C (Table S1). The Y-structure substrate was prepared by annealing X12-3* and X12-4 NC oligonucleotides (Cejka and Kowalczykowski, 2010) (Table S1). MRN degradation assays on pRF substrates were conducted more than 3 times and MR degradation assays on dsDNA and splayed arm substrates were performed twice.

Western blotting—Cells were collected by trypsinization and lysed in RIPA lysis buffer (150 mM NaCl, 1.0% IGEPAL CA-630, 0.5% sodium deoxycholate, 0.1% SDS, 50 mM Tris base, pH 8.0). Phosphatase and protease inhibitors (Gold Biotechnology) were added freshly

to the lysis buffer. Following gel electrophoresis and transfer of cell extracts onto nitrocellulose, membranes were incubated for 1 hr or overnight in blocking buffer (5% milk in TBS + 0.1% tween). Membranes were subsequently incubated with primary antibodies diluted in antibody buffer (3% BSA in TBS + 0.1% tween) for 2 hrs at room temperature or overnight at 4°C. Detection was achieved using appropriate horseradish peroxidase (HRP)-conjugated secondary antibodies. Anti-ZRANB3 (1:5,000, Bethyl Laboratories), anti-SMARCAL1 (1:1,000, Santa Cruz Biotechnology), anti-BRCA1 (1:500, Bethyl Laboratories), anti-BRCA2 (1:1,000, Bethyl Laboratories), anti-vinculin (1:100,000, Sigma-Aldrich), anti-β-actin (1:100,000, Novus Biologicals), anti-GAPDH (1:5,000, Novus Biologicals), anti-HLTF (1:2,000, Abcam), anti-LAMIN B1 (Thermo Fisher Scientific), anti-FANCD2 (1:1,000, Novus Biologicals), anti-PCNA (1:100,000, Abcam), anti-NBS1 (GeneTex), anti-MRE11 (Cell Signaling Technology), anti-RPA2 (Bethyl Laboratories) antibodies were used in western blot experiments.

Protein immunoprecipitation—HEK293T cells stably expressing pMSCV-HA-GFP, pMSCV-HA-SMARCAL1 and pMSCV-HA-RPA2 (Ciccia et al., 2009), pMSCV-HA-ZRANB3 (Ciccia et al., 2012), pMSCV-HA-MRE11 and pMSCV-HA-NBS1 (Ciccia et al., 2014), pMSCV-HA-SMARCAL1-$\Delta N_{1\text{-}115}$ were treated with 2 mM HU or left untreated for 5 hrs. Cells were then collected in cold PBS, pelleted by centrifugation and resuspended in the following lysis buffer: 50 mM Tris-HCl pH 7.5, 1% NP-40 and 150 mM NaCl supplemented with 1X protease inhibitor cocktail (ProBlock Gold, Gold Biotechnology), 1X phosphatase inhibitor cocktail (Simple Stop 1, Gold Biotechnology), 2 mM $MgCl_2$ and 125 U/ml Benzonase (Santa Cruz). Following incubation for 30 min at 4°C with gentle agitation, cell lysates were cleared by centrifugation and the supernatant collected (input). Cleared supernatants were then incubated with anti-HA-agarose beads (Sigma-Aldrich) for 4 hrs at 4°C with gentle agitation. Beads were subsequently washed three times in buffer (50 mM Tris-HCl pH 7.4, 1% NP-40 and 150 mM NaCl), resuspended in sample buffer (50 mM Tris-HCl pH 6.8, 2% SDS and 1.7 M β-mercaptoethanol in PBS) and boiled to elute bound proteins.

In vitro pulldowns—WT and $NZF_{\text{-zinc}}$-mutant ZRANB3 proteins purified from *Sf*9 insect cells as described (Ciccia et al., 2012) were re-bound to EZview red anti-FLAG M2 beads (Sigma-Aldrich) and subsequently incubated with purified unmodified PCNA (75 ng) and polyubiquitinated PCNA (150 ng) (gifts from Lajos Haracska) in 100 µL of FLAG binding buffer (50 mM Tris pH 8, 400 mM NaCl, 10% glycerol, 0.1% Triton X-100). After 4 hrs of gentle agitation at 4°C, beads were washed 4 times with FLAG binding buffer and analyzed by gel electrophoresis and western blotting.

Kaplan-Meier analysis—For 2,272 METABRIC cases available from cBioPortal with "Cancer Type Detailed" values of "Breast Invasive Ductal Carcinoma" (1,500 cases) or "Invasive Breast Carcinoma" (772 additional cases), we retrieved clinical data, *SMARCAL1* mRNA expression z-scores from microarray, and somatic mutation calls from cBioPortal. Data was retrieved on May 24, 2017. *SMARCAL1* expression data was missing for 599 cases, leaving 1,673 cases for Kaplan-Meier analysis based on *SMARCAL1* expression. Low *SMARCAL1* expression was defined as z-scores less than -1. *BRCA1* mutations

excluded variants classified as “silent” or “splice site region”. Kaplan-Meier curves for overall survival were calculated using the Surv() function, log-rank tests comparing survival curves calculated using the survdiff() function with rho = 0 [survdiff(Surv(time = OS_MONTHS, event = delta) ~ class_label, rho = 0)], and survival curves plotted using the survfit() function. All functions are from the survival package in R.

QUANTIFICATION AND STATISTICAL ANALYSIS

Statistical differences in PLA and RAD51 foci experiments, comet and chromosomal aberrations assays were determined by one-way ANOVA test without multiple comparison correction (Fisher’s LSD test). Nascent DNA degradation and cell survival experiments were analyzed by Mann–Whitney test and Student’s t-test, respectively. Statistical analysis was performed using GraphPad Prism software (Version 6.0). In all cases: n.s. $p>0.05$; * $p<0.05$; ** $p<0.01$; *** $p<0.001$; **** $p<0.0001$.

DATA AND SOFTWARE AVAILABILITY

All data is available by request to the corresponding author. Raw images have been deposited in Mendeley Data and are available at http://dx.doi.org/10.17632/pjtrfbmsv7.1.

Supplementary Material

Refer to Web version on PubMed Central for supplementary material.

Acknowledgments

We thank Dr. Richard Baer for discussions and comments on the manuscript. This work was supported by the Ines Mandl research fellowship and NIH training grant 4T32CA009503-30 (to J.W.H), NIH fellowship F31CA210607 (to C.M.), NIH grant R01CA197774, Breast Cancer Alliance young investigator grant, Ovarian Cancer Research Fund Alliance Liz Tilberis award 368964 and Susan G. Komen career catalyst research grant CCR16377030 (to A.C.), AIRC-Associazione Italiana per Ricerca sul Cancro, European Research Council grant 614541 and Armenise-Harvard CDA (to V.C.), Swiss National Science foundation grant PP00P3_159323 and European Research Council grant 681630 (to P.C.). G.L. is supported by an American-Italian Cancer Foundation post-doctoral research fellowship and V.S. is funded by Fondazione Veronesi.

References

Achar YJ, Balogh D, Neculai D, Juhasz S, Morocz M, Gali H, Dhe-Paganon S, Venclovas C, Haracska L. Human HLTF mediates postreplication repair by its HIRAN domain-dependent replication fork remodelling. Nucleic Acids Res. 2015; 43:10277–10291. [PubMed: 26350214]

Ait Saada A, Teixeira-Silva A, Iraqui I, Costes A, Hardy J, Paoletti G, Freon K, Lambert SAE. Unprotected Replication Forks Are Converted into Mitotic Sister Chromatid Bridges. Mol Cell. 2017; 66:398–410. e394. [PubMed: 28475874]

Anand R, Ranjha L, Cannavo E, Cejka P. Phosphorylated CtIP Functions as a Co-factor of the MRE11-RAD50-NBS1 Endonuclease in DNA End Resection. Mol Cell. 2016; 64:940–950. [PubMed: 27889449]

Apostolou P, Fostira F. Hereditary breast cancer: the era of new susceptibility genes. BioMed research international. 2013; 2013:747318. [PubMed: 23586058]

Badu-Nkansah A, Mason AC, Eichman BF, Cortez D. Identification of a Substrate Recognition Domain in the Replication Stress Response Protein Zinc Finger Ran-binding Domain-containing Protein 3 (ZRANB3). J Biol Chem. 2016; 291:8251–8257. [PubMed: 26884333]

Bansbach CE, Betous R, Lovejoy CA, Glick GG, Cortez D. The annealing helicase SMARCAL1 maintains genome integrity at stalled replication forks. Genes Dev. 2009; 23:2405–2414. [PubMed: 19793861]

Betous R, Couch FB, Mason AC, Eichman BF, Manosas M, Cortez D. Substrate-selective repair and restart of replication forks by DNA translocases. Cell reports. 2013; 3:1958–1969. [PubMed: 23746452]

Betous R, Mason AC, Rambo RP, Bansbach CE, Badu-Nkansah A, Sirbu BM, Eichman BF, Cortez D. SMARCAL1 catalyzes fork regression and Holliday junction migration to maintain genome stability during DNA replication. Genes Dev. 2012; 26:151–162. [PubMed: 22279047]

Blastyak A, Hajdu I, Unk I, Haracska L. Role of double-stranded DNA translocase activity of human HLTF in replication of damaged DNA. Mol Cell Biol. 2010; 30:684–693. [PubMed: 19948885]

Cejka P, Kowalczykowski SC. The full-length Saccharomyces cerevisiae Sgs1 protein is a vigorous DNA helicase that preferentially unwinds holliday junctions. J Biol Chem. 2010; 285:8290–8301. [PubMed: 20086270]

Ciccia A, Bredemeyer AL, Sowa ME, Terret ME, Jallepalli PV, Harper JW, Elledge SJ. The SIOD disorder protein SMARCAL1 is an RPA-interacting protein involved in replication fork restart. Genes Dev. 2009; 23:2415–2425. [PubMed: 19793862]

Ciccia A, Huang JW, Izhar L, Sowa ME, Harper JW, Elledge SJ. Treacher Collins syndrome TCOF1 protein cooperates with NBS1 in the DNA damage response. Proc Natl Acad Sci U S A. 2014; 111:18631–18636. [PubMed: 25512513]

Ciccia A, Nimonkar AV, Hu Y, Hajdu I, Achar YJ, Izhar L, Petit SA, Adamson B, Yoon JC, Kowalczykowski SC, et al. Polyubiquitinated PCNA Recruits the ZRANB3 Translocase to Maintain Genomic Integrity after Replication Stress. Mol Cell. 2012; 47:396–409. [PubMed: 22704558]

Ciccia A, Symington LS. Stressing Out About RAD52. Mol Cell. 2016; 64:1017–1019. [PubMed: 27984741]

Ding X, Ray Chaudhuri A, Callen E, Pang Y, Biswas K, Klarmann KD, Martin BK, Burkett S, Cleveland L, Stauffer S, et al. Synthetic viability by BRCA2 and PARP1/ARTD1 deficiencies. Nature communications. 2016; 7:12425.

Dungrawala H, Bhat KP, Le Meur R, Chazin WJ, Ding X, Sharan SK, Wessel SR, Sathe AA, Zhao R, Cortez D. RADX Promotes Genome Stability and Modulates Chemosensitivity by Regulating RAD51 at Replication Forks. Mol Cell. 2017; 67:374–386. e375. [PubMed: 28735897]

Dungrawala H, Rose KL, Bhat KP, Mohni KN, Glick GG, Couch FB, Cortez D. The Replication Checkpoint Prevents Two Types of Fork Collapse without Regulating Replisome Stability. Mol Cell. 2015; 59:998–1010. [PubMed: 26365379]

Guarani V, Paulo J, Zhai B, Huttlin EL, Gygi SP, Harper JW. TIMMDC1/C3orf1 functions as a membrane-embedded mitochondrial complex I assembly factor through association with the MCIA complex. Mol Cell Biol. 2014; 34:847–861. [PubMed: 24344204]

Guillemette S, Serra RW, Peng M, Hayes JA, Konstantinopoulos PA, Green MR, Cantor SB. Resistance to therapy in BRCA2 mutant cells due to loss of the nucleosome remodeling factor CHD4. Genes Dev. 2015; 29:489–494. [PubMed: 25737278]

Hashimoto Y, Ray Chaudhuri A, Lopes M, Costanzo V. Rad51 protects nascent DNA from Mre11-dependent degradation and promotes continuous DNA synthesis. Nat Struct Mol Biol. 2010; 17:1305–1311. [PubMed: 20935632]

Higgs MR, Reynolds JJ, Winczura A, Blackford AN, Borel V, Miller ES, Zlatanou A, Nieminuszczy J, Ryan EL, Davies NJ, et al. BOD1L Is Required to Suppress Deleterious Resection of Stressed Replication Forks. Mol Cell. 2015; 59:462–477. [PubMed: 26166705]

Hishiki A, Hara K, Ikegaya Y, Yokoyama H, Shimizu T, Sato M, Hashimoto H. Structure of a Novel DNA-binding Domain of Helicase-like Transcription Factor (HLTF) and Its Functional Implication in DNA Damage Tolerance. J Biol Chem. 2015; 290:13215–13223. [PubMed: 25858588]

Huang F, Mazina OM, Zentner IJ, Cocklin S, Mazin AV. Inhibition of homologous recombination in human cells by targeting RAD51 recombinase. J Med Chem. 2012; 55:3011–3020. [PubMed: 22380680]

Kile AC, Chavez DA, Bacal J, Eldirany S, Korzhnev DM, Bezsonova I, Eichman BF, Cimprich KA. HLTF's Ancient HIRAN Domain Binds 3′ DNA Ends to Drive Replication Fork Reversal. Mol Cell. 2015; 58:1090–1100. [PubMed: 26051180]

Kolinjivadi AM, Sannino V, De Antoni A, Zadorozhny K, Kilkenny M, Techer H, Baldi G, Shen R, Ciccia A, Pellegrini L, et al. Smarcal1-Mediated Fork Reversal Triggers Mre11-Dependent Degradation of Nascent DNA in the Absence of Brca2 and Stable Rad51 Nucleofilaments. Mol Cell. 2017

Leuzzi G, Marabitti V, Pichierri P, Franchitto A. WRNIP1 protects stalled forks from degradation and promotes fork restart after replication stress. EMBO J. 2016; 35:1437–1451. [PubMed: 27242363]

Lomonosov M, Anand S, Sangrithi M, Davies R, Venkitaraman AR. Stabilization of stalled DNA replication forks by the BRCA2 breast cancer susceptibility protein. Genes and Dev. 2003; 17:3017–3022. [PubMed: 14681210]

Neelsen KJ, Chaudhuri AR, Follonier C, Herrador R, Lopes M. Visualization and interpretation of eukaryotic DNA replication intermediates in vivo by electron microscopy. Methods in molecular biology. 2014; 1094:177–208. [PubMed: 24162989]

Neelsen KJ, Lopes M. Replication fork reversal in eukaryotes: from dead end to dynamic response. Nat Rev Mol Cell Biol. 2015; 16:207–220. [PubMed: 25714681]

Pathania S, Bade S, Le Guillou M, Burke K, Reed R, Bowman-Colin C, Su Y, Ting DT, Polyak K, Richardson AL, et al. BRCA1 haploinsufficiency for replication stress suppression in primary cells. Nature communications. 2014; 5:5496.

Petruk S, Sedkov Y, Johnston DM, Hodgson JW, Black KL, Kovermann SK, Beck S, Canaani E, Brock HW, Mazo A. TrxG and PcG proteins but not methylated histones remain associated with DNA through replication. Cell. 2012; 150:922–933. [PubMed: 22921915]

Postow L, Woo EM, Chait BT, Funabiki H. Identification of SMARCAL1 as a component of the DNA damage response. J Biol Chem. 2009

Prakash R, Zhang Y, Feng W, Jasin M. Homologous recombination and human health: the roles of BRCA1, BRCA2, and associated proteins. Cold Spring Harb Perspect Biol. 2015; 7:a016600. [PubMed: 25833843]

Ray Chaudhuri A, Callen E, Ding X, Gogola E, Duarte AA, Lee JE, Wong N, Lafarga V, Calvo JA, Panzarino NJ, et al. Replication fork stability confers chemoresistance in BRCA-deficient cells. Nature. 2016; 535:382–387. [PubMed: 27443740]

Sato K, Shimomuki M, Katsuki Y, Takahashi D, Kobayashi W, Ishiai M, Miyoshi H, Takata M, Kurumizaka H. FANCI-FANCD2 stabilizes the RAD51-DNA complex by binding RAD51 and protects the 5′-DNA end. Nucleic Acids Res. 2016; 44:10758–10771. [PubMed: 27694619]

Schlacher K, Christ N, Siaud N, Egashira A, Wu H, Jasin M. Double-strand break repair-independent role for BRCA2 in blocking stalled replication fork degradation by MRE11. Cell. 2011; 145:529–542. [PubMed: 21565612]

Schlacher K, Wu H, Jasin M. A distinct replication fork protection pathway connects Fanconi anemia tumor suppressors to RAD51-BRCA1/2. Cancer Cell. 2012; 22:106–116. [PubMed: 22789542]

Sims AE, Spiteri E, Sims RJ 3rd, Arita AG, Lach FP, Landers T, Wurm M, Freund M, Neveling K, Hanenberg H, et al. FANCI is a second monoubiquitinated member of the Fanconi anemia pathway. Nat Struct Mol Biol. 2007; 14:564–567. [PubMed: 17460694]

Tan SLW, Chadha S, Liu Y, Gabasova E, Perera D, Ahmed K, Constantinou S, Renaudin X, Lee M, Aebersold R, et al. A Class of Environmental and Endogenous Toxins Induces BRCA2 Haploinsufficiency and Genome Instability. Cell. 2017; 169:1105–1118. e1115. [PubMed: 28575672]

Unk I, Hajdu I, Blastyak A, Haracska L. Role of yeast Rad5 and its human orthologs, HLTF and SHPRH in DNA damage tolerance. DNA Repair (Amst). 2010; 9:257–267. [PubMed: 20096653]

Vujanovic M, Krietsch J, Raso MC, Terraneo N, Zellweger R, Schmid JA, Taglialatela A, Huang JW, Holland CL, Zwicky K, et al. Replication Fork Slowing and Reversal upon DNA Damage Require PCNA Polyubiquitination and ZRANB3 DNA Translocase Activity. Mol Cell. 2017; 67:882–890. e885. [PubMed: 28886337]

Wang AT, Kim T, Wagner JE, Conti BA, Lach FP, Huang AL, Molina H, Sanborn EM, Zierhut H, Cornes BK, et al. A Dominant Mutation in Human RAD51 Reveals Its Function in DNA

Interstrand Crosslink Repair Independent of Homologous Recombination. Mol Cell. 2015; 59:478–490. [PubMed: 26253028]

Weston R, Peeters H, Ahel D. ZRANB3 is a structure-specific ATP-dependent endonuclease involved in replication stress response. Genes Dev. 2012; 26:1558–1572. [PubMed: 22759634]

Yuan J, Ghosal G, Chen J. The annealing helicase HARP protects stalled replication forks. Genes Dev. 2009; 23:2394–2399. [PubMed: 19793864]

Yuan J, Ghosal G, Chen J. The HARP-like Domain-Containing Protein AH2/ZRANB3 Binds to PCNA and Participates in Cellular Response to Replication Stress. Mol Cell. 2012; 47:410–421. [PubMed: 22705370]

Yusufzai T, Kong X, Yokomori K, Kadonaga JT. The annealing helicase HARP is recruited to DNA repair sites via an interaction with RPA. Genes Dev. 2009; 23:2400–2404. [PubMed: 19793863]

Zellweger R, Dalcher D, Mutreja K, Berti M, Schmid JA, Herrador R, Vindigni A, Lopes M. Rad51-mediated replication fork reversal is a global response to genotoxic treatments in human cells. J Cell Biol. 2015; 208:563–579. [PubMed: 25733714]

HIGHLIGHTS

- SNF2 fork remodelers promote nascent DNA degradation in BRCA1/2-deficient cells
- Fork remodelers favor MRE11 binding to stalled forks in BRCA1-deficient cells
- Forks regressed by fork remodelers are degraded by MRE11 in BRCA1-deficient cells
- Depletion of fork remodelers reduces genomic instability in BRCA1/2-deficient cells

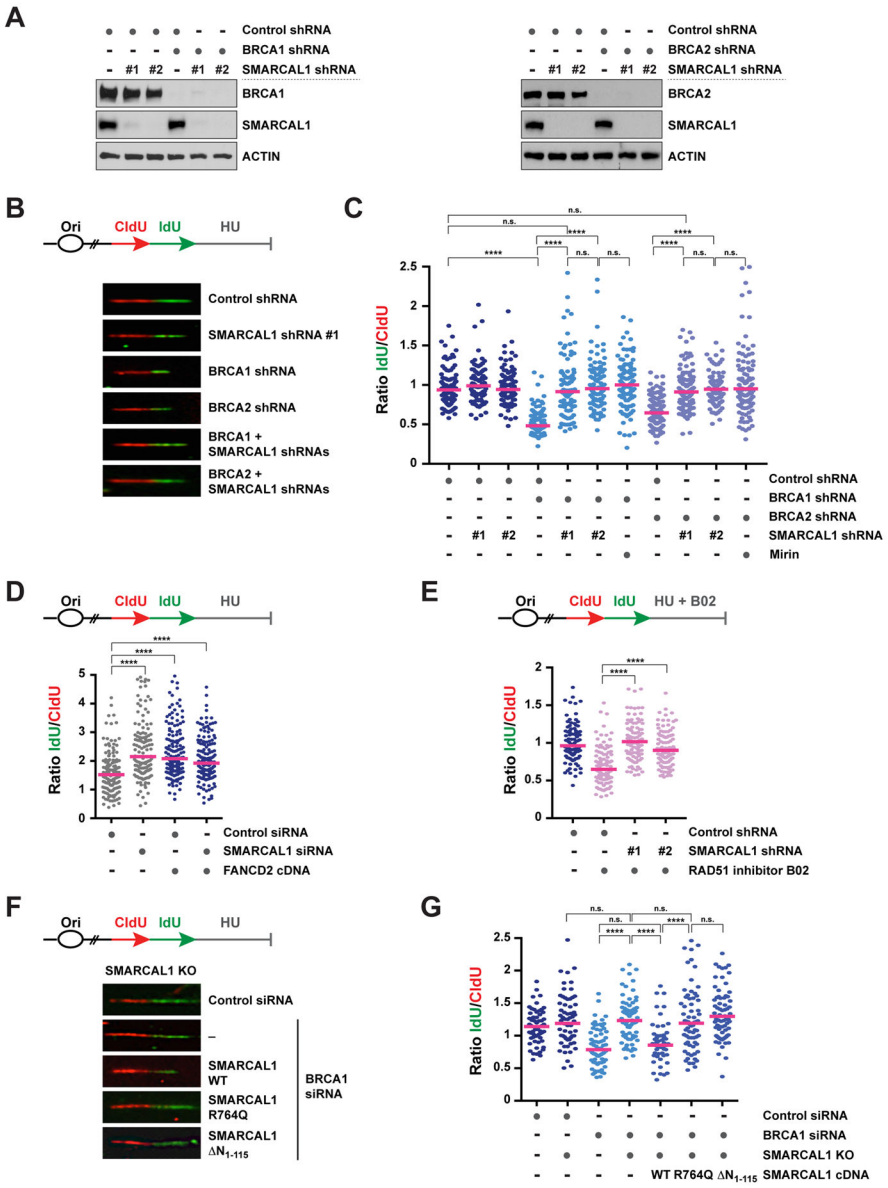

Figure 1. Analysis of nascent DNA degradation in BRCA1/2- and FANCD2-deficient cells upon SMARCAL1 depletion

(A) Detection by western blot of BRCA1 (left), BRCA2 (right) and SMARCAL1 protein levels in MCF10A cells subjected to shRNA-dependent depletion. β-actin levels are shown as loading controls.

(B) Schematic of CldU/IdU pulse-labeling followed by a 5 hr hydroxyurea (HU; 2 mM) treatment (top). Representative images of CldU and IdU replication tracks in HU-treated MCF10A cells expressing the indicated shRNAs (bottom).

(C) Dot plot of IdU to CldU tract length ratios for individual replication forks in HU-treated MCF10A cells expressing the indicated shRNAs with or without mirin (50 μM). The median value of 200 or more IdU and CldU tracts per experimental condition is indicated. Statistical analysis was conducted using Mann-Whitney test (n.s. not significant, **** $p<0.0001$). Data are representative of 3 independent experiments.

(D) Schematic of CldU/IdU pulse-labeling followed by HU treatment as in (B) (top) and dot plot of IdU to CldU tract length ratios for individual replication forks in HU-treated PD20 cells with or without complementation with FANCD2 cDNA and treatment with SMARCAL1 siRNA (bottom). Data are shown and analyzed as in (C) and represent 2 independent experiments.
(E) Schematic of the CldU/IdU pulse-labeling assay (top) and dot plot of IdU to CldU tract length ratios for individual replication forks in MCF10A cells with or without combined treatment with HU (2 mM) and B02 (25 μM) for 5 hrs (bottom). Data are shown and analyzed as in (C) and represent 2 independent replicates.
(F) Schematic of the CldU/IdU pulse-labeling assay conducted as in (B) (top) in control and SMARCAL1 KO MCF10A cells subjected to control or BRCA1 siRNA treatment with or without expression of wild-type (WT), R764Q- or $\Delta N_{1\text{-}115}$-mutant SMARCAL1 proteins. Representative images of CldU (red) and IdU (green) replication tracks in the MCF10A cells indicated above after HU treatment (bottom).
(G) Dot plot of IdU to CldU tract length ratios for individual replication forks in the MCF10A cells shown in (F) after HU treatment. Data are shown and analyzed as in (C) and represent 2 independent experiments. See also Figure S1.

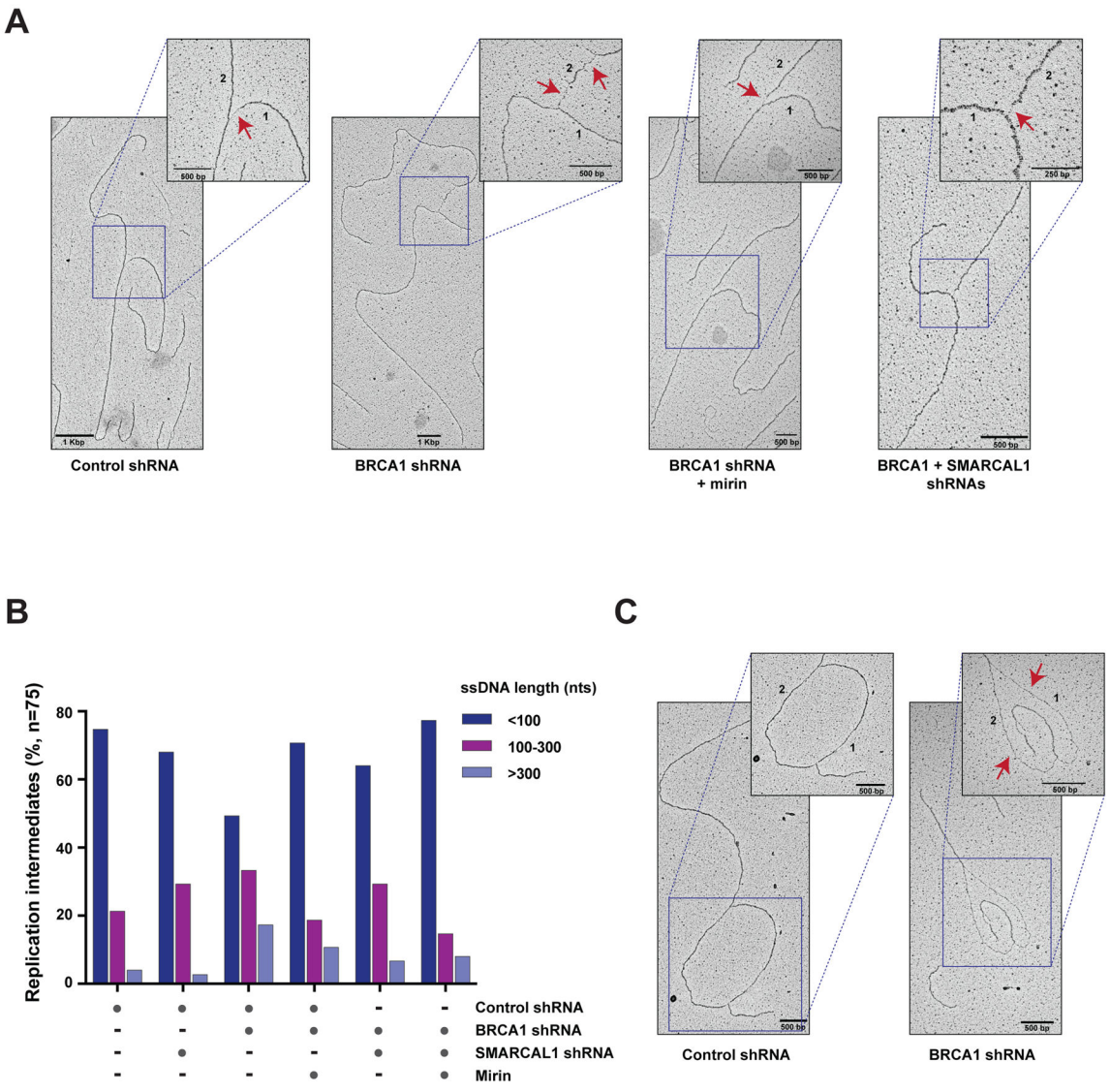

Figure 2. Electron microscopy analysis of replication intermediates in BRCA1- and/or SMARCAL1-depleted cells

(A) Representative images of replication intermediates detected by electron microscopy upon a 5 hr HU treatment (2 mM) of control, BRCA1- and/or SMARCAL1-depleted MCF10A cells with or without mirin (50 μM). Replication fork arms and ssDNA gaps are indicated by numbers (i.e., 1 and 2) and arrows, respectively.

(B) Bar graph representation of the percentage of replication intermediates with ssDNA regions of the indicated length in BRCA1- and/or SMARCAL1-depleted MCF10A cells treated as described in (A). 75 replication intermediates were analyzed per condition. Similar results were obtained in an independent experiment (Figure S2A).

(C) Representative images of replication fork bubbles detected by electron microscopy in HU-treated control and BRCA1-depleted MCF10A cells. Replication fork arms and ssDNA gaps are indicated as in (A). See also Figure S2.

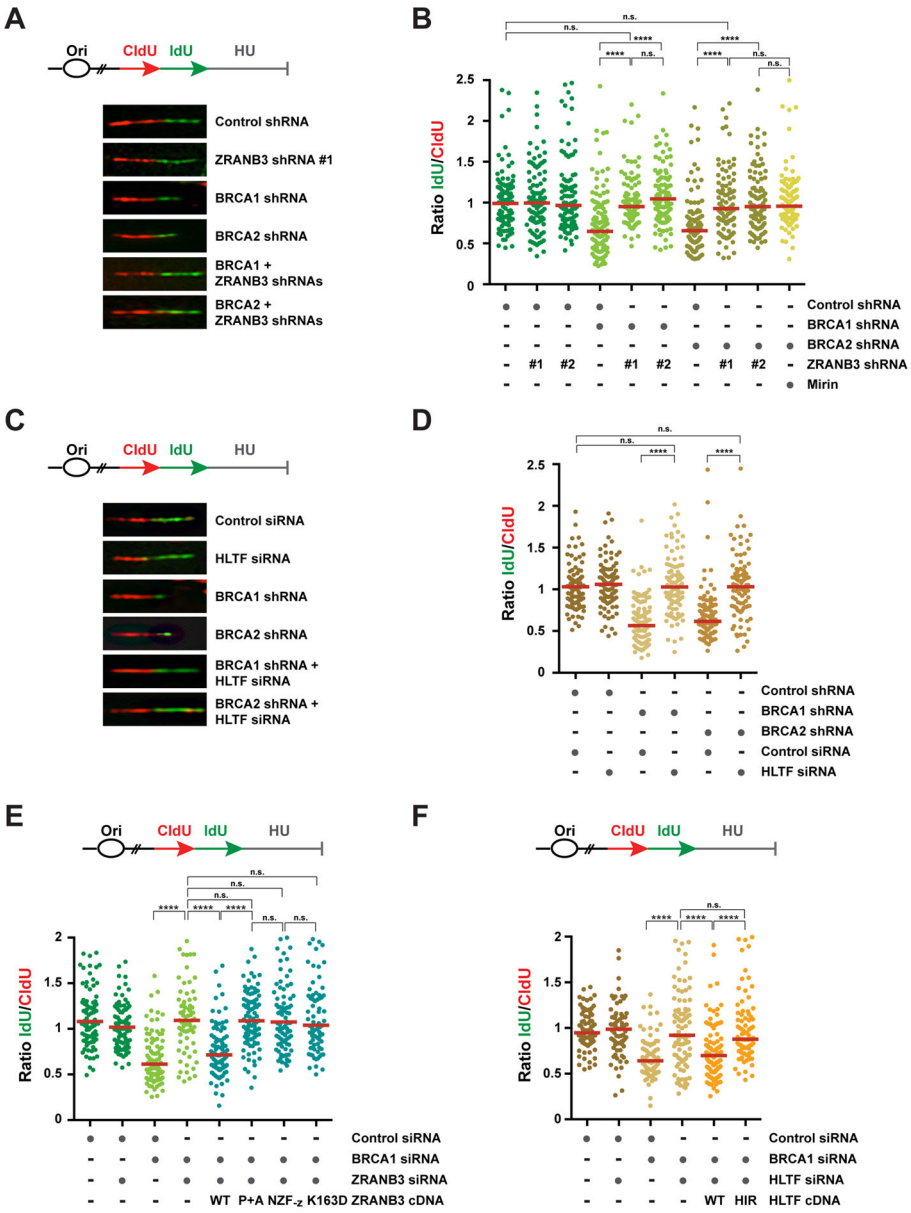

Figure 3. Measurement of nascent DNA degradation in BRCA1/2-deficient cells following depletion of ZRANB3 or HLTF

(A) Schematic of CldU/IdU pulse-labeling followed by a 5 hr HU treatment (2 mM) (top) and representative images of CldU and IdU replication tracks in HU-treated MCF10A expressing the indicated shRNAs (bottom).

(B) Dot plot of IdU to CldU tract length ratios for individual replication forks in the HU-treated MCF10A cells shown in (A) with or without mirin (50 μM). The median value of 200 or more IdU and CldU tracts per experimental condition is indicated. P-values were calculated by Mann-Whitney test (n.s. not significant, **** p<0.0001). Data are representative of 2 independent experiments.

(C) Schematic of CldU/IdU pulse-labeling followed by HU treatment as in (A) (top) and representative images of CldU and IdU replication tracks in HU-treated MCF10A expressing the indicated sh/siRNAs (bottom).
(D) Dot plot of IdU to CldU tract length ratios for individual replication forks in the HU-treated MCF10A cells shown in (C). The experiment was conducted as in (B). Data are representative of 2 independent experiments and p-values were calculated as in (B).
(E) Schematic of the CldU/IdU pulse-labeling assay conducted as described in (A) (top) and dot plot of IdU to CldU tract length ratios for individual replication forks in HU-treated MCF10A cells with or without BRCA1 and/or ZRANB3 siRNA-mediated depletion (bottom). ZRANB3-depleted cells were reconstituted with siRNA-resistant WT, PIP+APIM (P+A)-, NZF_{-zinc} (NZF_{-z})- or K163D-mutant ZRANB3 proteins. Data are shown and analyzed as in (B) and represent 2 independent experiments.
(F) Schematic of the CldU/IdU pulse-labeling assay performed as indicated in (A) (top) and dot plot of IdU to CldU tract length ratios for individual replication forks in HU-treated MCF10A cells with or without BRCA1 and/or HLTF siRNA-mediated depletion (bottom). HLTF-depleted cells were reconstituted with siRNA-resistant WT and HIRAN (HIR)-mutant HLTF proteins. Data are shown and analyzed as in (B) and represent 2 independent experiments. See also Figure S3.

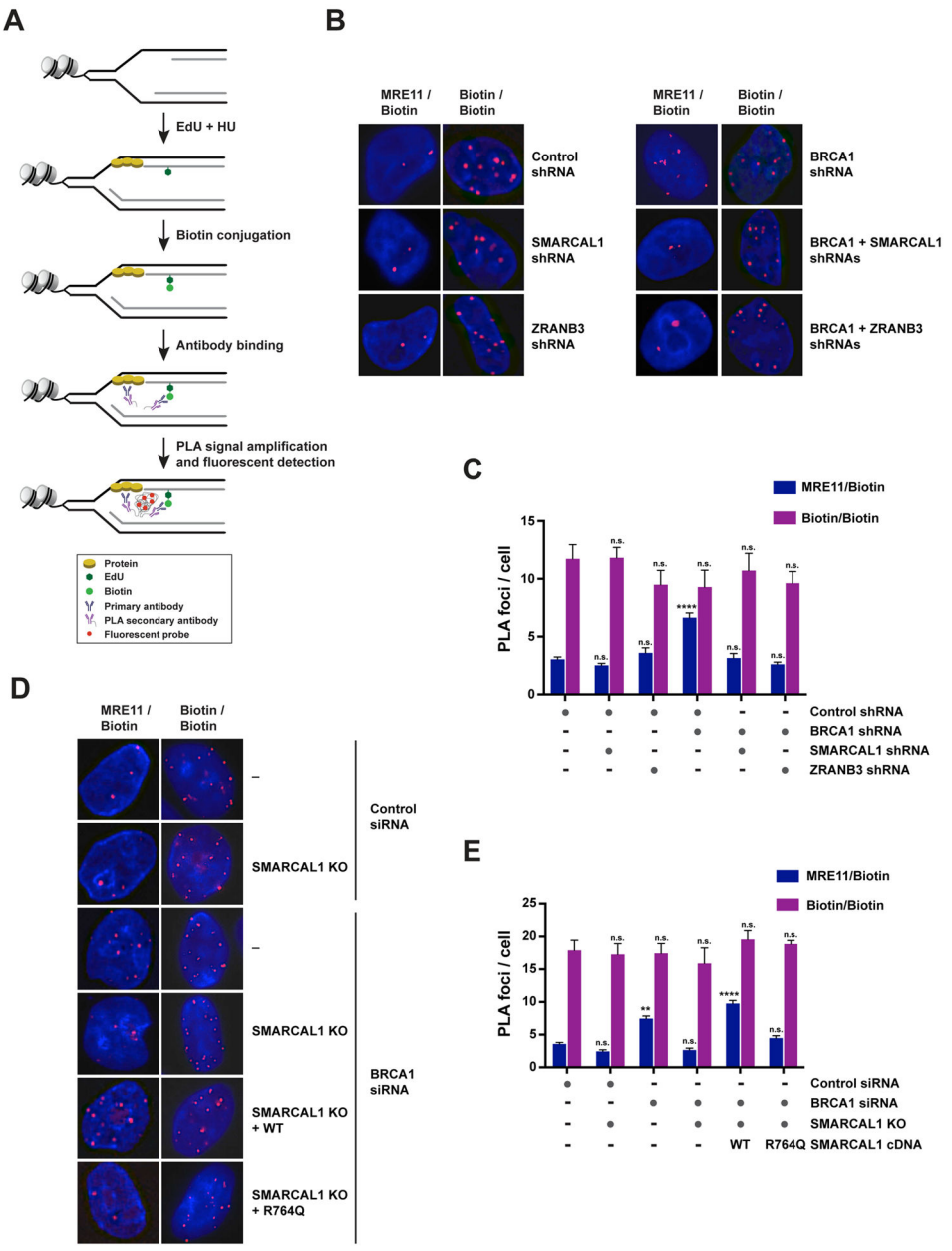

Figure 4. Detection of MRE11 association with nascent DNA in BRCA1-deficient cells upon depletion of SMARCAL1 or ZRANB3

(A) Schematic of the proximity ligation assay (PLA) utilized to detect the association of proteins with nascent DNA, as described in the main text.

(B) Representative images of PLA foci obtained in the indicated HU-treated MCF10A cells upon incubation with anti-MRE11 and anti-biotin antibodies (MRE11/Biotin; left) or with two distinct anti-biotin antibodies (Biotin/Biotin; right) according to the protocol depicted in (A). Each red spot corresponds to an interaction. DNA was stained with DAPI (blue).

(C) Representation of the mean + SEM of the number of MRE11/Biotin (blue) PLA foci per cell (≥ 2 foci) in HU-treated MCF10A cells upon depletion of the factors indicated in (B). The mean + SEM of the number of Biotin/Biotin (purple) PLA foci per cell (≥ 2 foci) was

used as control for the number of replication sites in each condition. 100–300 cells were analyzed per condition. Statistical analysis was conducted using one-way ANOVA on each sample relative to control samples (n.s., not significant; **** $p<0.0001$). Data are representative of 2 independent replicates.
(D) Representative images of PLA foci obtained from HU-treated control or SMARCAL1 KO MCF10A cells as shown in (B). Cells were subjected or not to BRCA1 siRNA-mediated depletion and reconstitution with WT or R764Q-mutant SMARCAL1 proteins.
(E) Representation of the mean + SEM of the number of MRE11/Biotin (blue) and Biotin/Biotin (purple) PLA foci per cell (≥ 2 foci) in HU-treated control and SMARCAL1 KO MCF10A cells, as shown in (D). 100–300 cells were analyzed per condition. Statistical analysis was conducted as in (C) (n.s. not significant; ** $p<0.01$; **** $p<0.0001$). Data are representative of 2 independent replicates. See also Figure S4.

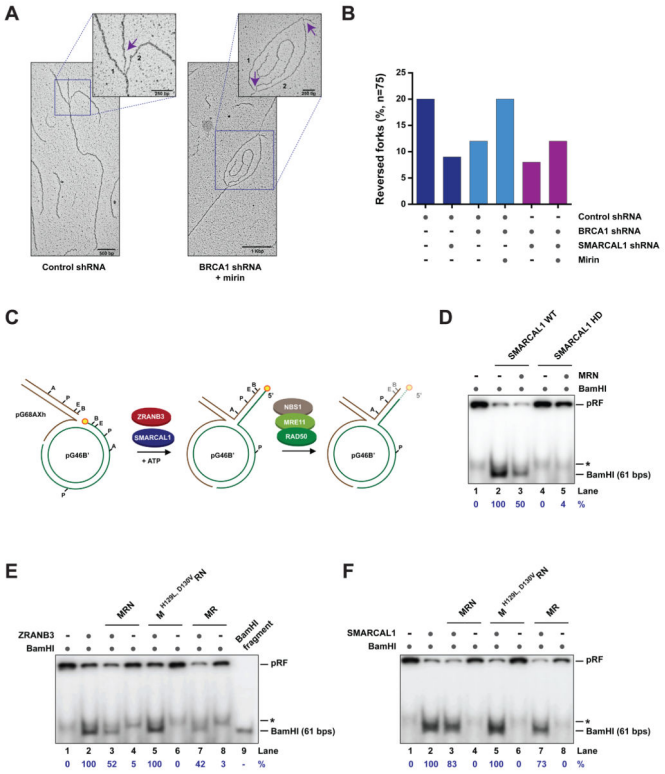

Figure 5. Nucleolytic activity of MRE11 on reversed fork structures

(A) Representative images of reversed fork intermediates detected by electron microscopy upon a 5 hr HU treatment (2 mM) of control and BRCA1-depleted MCF10A cells with or without mirin (50 μM). Parental and reversed fork arms are indicated by numbers (i.e., 1 and 2) and arrows, respectively.

(B) Representation of the percentage of reversed fork intermediates detected by electron microscopy in HU-treated BRCA1- and/or SMARCAL1-depleted MCF10A cells with or without mirin treatment, as described in (A). 75 replication intermediates were analyzed per condition. Similar results were obtained in an independent experiment (Figure S5B).

(C) Schematic of the fork reversal and degradation assay utilized to monitor the activity of MRN or MR complexes on reversed fork structures generated on a plasmid-sized replication fork (pRF) by SMARCAL1 or ZRANB3, as described in the main text.

(D) Fork reversal and degradation assay conducted upon incubation of the pRF substrate with wild-type (WT, 50 nM) or helicase-dead (HD, 50 nM) SMARCAL1 proteins for 5 min with or without subsequent addition of MRN complex (50 nM) for 2 hrs. Quantification of the BamHI digestion of reversed fork products is shown underneath each lane. The asterisk indicates a non-specific band. Similar results were obtained in an independent experiment.

(E–F) Fork reversal and degradation assay conducted upon incubation of the pRF substrate with ZRANB3 or SMARCAL1 proteins (50 nM) for 5 min with or without subsequent addition of WT or nuclease deficient ($M^{H129L,D130V}RN$) MRN or MR complex (50 nM) for 2 hrs. dsDNA corresponding to the BamHI digestion product of pRF was utilized as a marker in (E). Detection and quantification of BamHI digestion products was conducted as in (D). Data are representative of 3 or more independent experiments.

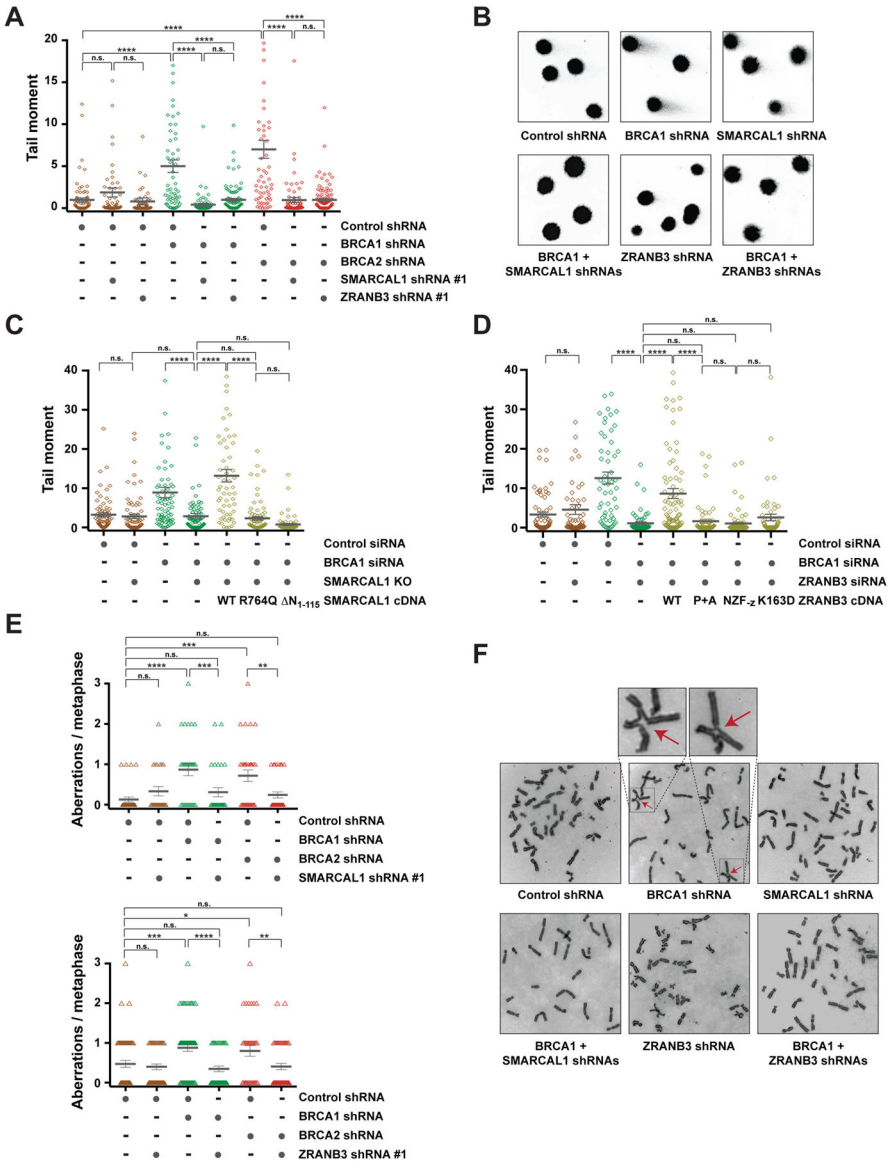

Figure 6. Effects of the depletion of SNF2-family members on genomic stability in BRCA1/2-deficient cells

(A) Dot plot of neutral comet tail moments detected in MCF10A cells expressing the indicated shRNAs following a 100 nM camptothecin (CPT) treatment for 5 hrs. Data are represented as the mean ± SEM of 75 or more comet tails per indicated condition. P-values were calculated by one-way ANOVA (n.s. not significant, **** $p<0.0001$). Data are representative of 2 independent experiments.

(B) Representative images of neutral comet tails from CPT-treated MCF10A cells expressing the indicated shRNAs.

(C) Dot plot of neutral comet tail moments detected upon a 5 hr CPT treatment (100 nM) of control or SMARCAL1 KO MCF10A cells with or without BRCA1 siRNA-mediated depletion and reconstitution with WT, R764Q- or ΔN_{1-115}-mutant SMARCAL1 proteins. Data are shown and analyzed as in (A) and represent 2 independent replicates.

(D) Dot plot of neutral comet tail moments upon a 5 hr CPT treatment (100 nM) of MCF10A cells with or without BRCA1 and/or ZRANB3 siRNA-mediated depletion and reconstitution with siRNA-resistant WT, PIP+APIM (P+A)-, NZF_{-zinc} (NZF_{-z})- or K163D-mutant ZRANB3 proteins. Data are shown and analyzed as in (A) and represent 2 independent experiments.
(E) Analysis of chromosomal aberrations in MCF10A cells expressing the indicated shRNAs upon a 100 nM CPT treatment for 5 hrs. Data are represented as the mean ± SEM of 25 or more metaphases per indicated condition. P-values were calculated by one-way ANOVA (n.s. not significant, ** $p<0.01$, *** $p<0.001$, **** $p<0.0001$). Data are representative of 2 independent experiments.
(F) Representative images of metaphase spreads from CPT-treated MCF10A cells expressing the indicated shRNAs. Chromosomal aberrations are indicated by arrows. See also Figure S6.

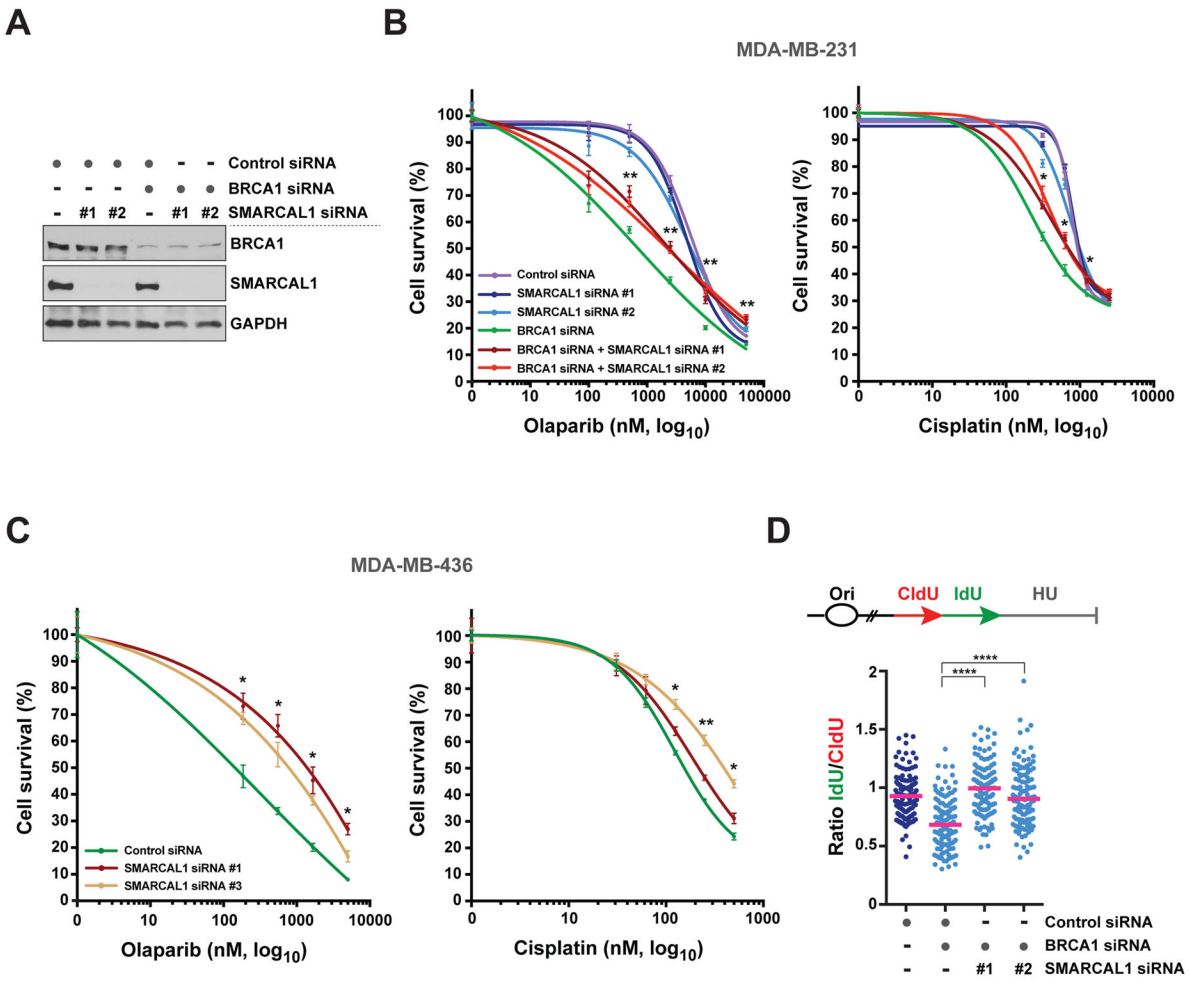

Figure 7. Analysis of cell survival in BRCA1-deficient breast cancer cells upon SMARCAL1 depletion

(A) Western blot showing BRCA1 and SMARCAL1 protein levels in MDA-MB-231 cells transfected with the indicated siRNAs. GAPDH levels are shown as loading controls.

(B) Survival analysis in MDA-MB-231 cells subjected to BRCA1 and/or SMARCAL1 depletion with two independent siRNAs, as indicated in (A), upon treatment with olaparib (left) or cisplatin (right). Cell survival is expressed as percentage relative to the untreated control and data represent the mean ± SD of at least 3 replicates per condition. Asterisks indicate p-values that are significant for both SMARCAL1/BRCA1 co-depleted samples (#1 and #2) relative to their corresponding BRCA1-depleted sample (unpaired Student's t-test; * $p<0.05$; ** $p<0.01$). Data are representative of 2 independent experiments.

(C) Survival analysis in BRCA1-mutant MDA-MB-436 cells subjected to SMARCAL1 depletion with 2 independent siRNAs upon treatment with olaparib (left) or cisplatin (right). Data are represented as in (B). Asterisks indicate p-values that are significant for both SMARCAL1-depleted samples (#1 and #2) relative to their corresponding control (unpaired Student's t-test; * $p<0.05$; ** $p<0.01$). Data are representative of 2 independent experiments.

(D) Schematic of the CldU/IdU pulse-labeling assay (top) and dot plot of IdU to CldU tract length ratios for individual replication forks in MDA-MB-231 cells treated with HU (2 mM

for 5 hrs) and the indicated siRNAs (bottom). The median value of 200 or more IdU and CldU tracts per experimental condition is indicated. Statistical analysis was conducted using Mann-Whitney test (**** $p<0.0001$). Data are representative of 2 independent experiments. See also Figure S7.

KEY RESOURCES TABLE

REAGENT or RESOURCE	SOURCE	IDENTIFIER
Antibodies		
Rat polyclonal anti-BrdU (DNA fiber assay)	AbD Serotec	Cat#MCA2060T; RRID:AB_10015293
Mouse monoclonal anti-BrdU (DNA fiber assay)	Becton Dickinson	Cat#347580; RRID: AB_10015219
Mouse monoclonal anti-MRE11 (PLA)	GeneTex	Cat#GTX70212; RRID:AB_372398
Rabbit polyclonal anti-biotin (PLA)	Bethyl Laboratories	Cat#A150-109A; RRID:AB_67327
Mouse monoclonal anti-biotin (PLA)	Jackson ImmunoResearch	Cat#200-002-211; RRID:AB_2339006
Mouse monoclonal anti-RPA2 (PLA)	Thermo Fisher Scientific	Cat#MA1-26418; RRID:AB_795362
Mouse monoclonal anti-γH2AX (PLA)	BioLegend	Cat#613402; RRID:AB_315795
Mouse monoclonal anti-PCNA (PLA)	Thermo Fisher Scientific	Cat#MA5-11358; RRID:AB_10982348
Rabbit polyclonal anti-ZRANB3	Bethyl Laboratories	Cat#A303-033A; RRID:AB_10773114
Mouse monoclonal anti-SMARCAL1	Santa Cruz Biotechnologies	Cat#sc-376377; RRID:AB_10987841
Rabbit polyclonal anti-BRCA1	Bethyl Laboratories	Cat#A301-378A; RRID:AB_937737
Rabbit polyclonal anti-BRCA2	Bethyl Laboratories	Cat#A303-434A; RRID:AB_10952240
Mouse monoclonal anti-vinculin	Sigma-Aldrich	Cat#V9131; RRID:AB_477629
Rabbit polyclonal anti-β-actin	Novus Biologicals	Cat#NB600-503; RRID:AB_10077516
Mouse monoclonal anti-GAPDH	Novus Biologicals	Cat#NB300-221; RRID:AB_10077627
Rabbit polyclonal anti-HLTF	Abcam	Cat#ab17984; RRID:AB_444160
Rabbit polyclonal anti-LAMIN B1	Thermo Fisher Scientific	Cat#PA5-19468; RRID:AB_10985414
Rabbit polyclonal anti-FANCD2	Novus Biologicals	Cat#NB100-182; RRID:AB_10002867
Rabbit polyclonal anti-PCNA	Abcam	Cat#ab18197; RRID:AB_444313
Mouse monoclonal anti-NBS1	GeneTex	Cat#GTX70224; RRID:AB_372445
Rabbit polyclonal anti-MRE11	Cell Signaling Technology	Cat#4895S; RRID:AB_10693926
Rabbit polyclonal anti-RPA2	Bethyl Laboratories	Cat#A300-244A; RRID:AB_185548
Rabbit polyclonal anti-RAD51 (IF)	CosmoBio	Cat#BAM-70-001-EX; RRID:AB_10708901

REAGENT or RESOURCE	SOURCE	IDENTIFIER
Goat anti-rat Alexa Fluor 594	Thermo Fisher Scientific	Cat#A-11007; RRID:AB_141374
Goat anti-mouse Alexa Fluor 488	Thermo Fisher Scientific	Cat#A-11029; RRID:AB_138404
Goat anti-rabbit Alexa Fluor 488	Thermo Fisher Scientific	Cat#A-11008; RRID:AB_143165
Bacterial and Virus Strains		
Subcloning Efficiency DH5α	Thermo Fisher Scientific	Cat#18265-017
Chemicals, Peptides, and Recombinant Proteins		
Transfection reagent: TransIT-293	Mirus	Cat#MIR 2700
Transfection reagent: Lipofectamine 3000	Thermo Fisher Scientific	Cat#L3000-008
Transfection reagent: Lipofectamine RNAiMAX	Thermo Fisher Scientific	Cat#13778-150
Puromycin	Gold Biotechnology	Cat#P-600-100
Blasticidin	Gold Biotechnology	Cat#B-800-100
CldU	Sigma-Aldrich	Cat#C6891
IdU	Sigma-Aldrich	Cat#I7125
EdU	Thermo Fisher Scientific	Cat#A10044
Hydroxyurea	Sigma-Aldrich	Cat#H8627
Camptothecin	Sigma-Aldrich	Cat#C9911
Mirin	Sigma-Aldrich	Cat#M9948
RAD51 inhibitor (B02)	Sigma-Aldrich	Cat#SML0364
Trimethylpsoralen	Sigma-Aldrich	Cat#T6137
BND-cellulose resin	Sigma-Aldrich	Cat#B6385
Amicon Ultra-0.5 Centrifugal Filter Unit with Ultracel-100	Millipore	Cat#UFC510096
Prolong Gold Antifade	Thermo Fisher Scientific	Cat#P36930
GelRed	Biotium	Cat#41002
Ethidium Bromide	Sigma-Aldrich	Cat#E1510
KaryoMAX Colcemid	Thermo Fisher Scientific	Cat#15210040
Giemsa	Sigma-Aldrich	Cat#G5637
Olaparib	SelleckChem	Cat#AZD2281
Biotin-azide	Thermo Fisher Scientific	Cat#B10184
Protease inhibitor cocktail	Sigma-Aldrich	Cat#P8340
Anti-FLAG M2 affinity gel	Sigma-Aldrich	Cat#A2220; RRID:AB_10063035
FLAG peptide	Sigma-Aldrich	Cat#F4799
CM sepharose resin	Sigma-Aldrich	Cat#CCF100
Anti-HA agarose beads	Sigma-Aldrich	Cat#A2095; RRID:AB_257974

REAGENT or RESOURCE	SOURCE	IDENTIFIER
EZview red anti-FLAG M2 beads	Sigma-Aldrich	Cat#F2426; RRID:AB_2616449
MRN/MR proteins	Anand et al., 2016	N/A
FLAG-SMARCAL1 protein	This study	N/A
FLAG-ZRANB3 protein	This study	N/A
PCNA and polyubiquitinated PCNA proteins	Gift from Lajos Haracska	N/A
Critical Commercial Assays		
Duolink In Situ Detection Reagents Red	Sigma-Aldrich	Cat#DUO92008
Duolink In Situ PLA Probe Anti-Rabbit MINUS	Sigma-Aldrich	Cat#DUO92005
Duolink In Situ PLA Probe Anti-Rabbit PLUS	Sigma-Aldrich	Cat#DUO92001
Deposited Data		
Unprocessed microscopy images, gels and blots	This paper; Mendeley Data	http://dx.doi.org/10.17632/pjtrfbmsv7.1
Experimental Models: Cell Lines		
MCF10A	ATCC	Cat#CRL-10317; RRID:CVCL_0598
hTERT-SD31	Ciccia et al., 2009	N/A
PD20	Sims et al., 2007	N/A
HEK293T	ATCC	Cat#CRL-11268; RRID:CVCL_1926
MDA-MB-231	ATCC	Cat#HTB-26; RRID:CVCL_0062
MDA-MB-436	ATCC	Cat#HTB-130; RRID:CVCL_0623
Oligonucleotides		
Table S1		
Recombinant DNA		
Plasmid: eSpCas9(1.1)	Addgene	Cat#71814
Plasmid: eCas9-P2A-Puro-gSMARCAL1ex3-1 (gRNA sequence: GCTCAGAGAGTGTAACGCCC)	This study	N/A
Plasmid: eCas9-P2A-Puro-gSMARCAL1ex3-2 (gRNA sequence: GTGAGAGCCATTTGACTACG)	This study	N/A
Plasmid: pG68A	Blastyak et al., 2010	N/A
Plasmid: pG46B	Blastyak et al., 2010	N/A
Plasmid: pDONR223-SMARCAL1	Ciccia et al., 2009	N/A
Plasmid: pDONR201-ZRANB3	Ciccia et al., 2012	N/A
Plasmid: pDONR223-HLTF	Orfeome v8.1 library	ID #100070304
Plasmid: pMSCV-PURO firefly shRNA (shRNA sequence: CCCGCCTGAAGTCTCTGATTAA)	Ciccia et al., 2012	N/A
Plasmid: pMSCV-PURO BRCA1 shRNA (shRNA sequence: GGCAGGTATTAGAAATGAA)	This study	N/A
Plasmid: pMSCV-PURO BRCA2 shRNA (shRNA sequence: CTCTTAGCTGTCTTAAAGA)	This study	N/A
Plasmid: pMSCV-BLAST SMARCAL1 shRNA #1	This study	N/A

REAGENT or RESOURCE	SOURCE	IDENTIFIER
(shRNA sequence: GGAACTCATTGCAGTGTTTAA)		
Plasmid: pMSCV-BLAST SMARCAL1 shRNA #2 (shRNA sequence: TGCCCTCATTCTCTTCTTCAAC)	This study	N/A
Plasmid: pMSCV-BLAST ZRANB3 shRNA #1 (shRNA sequence: CTGGATCAGACATCACACGATT)	This study	N/A
Plasmid: pMSCV-BLAST ZRANB3 shRNA #2 (shRNA sequence: CCGGATTCACATCTATACTAA)	This study	N/A
Plasmid: pHAGE-C-FLAG-HA-DEST	Guarani et al., 2014	N/A
Plasmid: pMSCV-N-HA-FLAG	Ciccia et al., 2009	N/A
Plasmid: pMSCV-HA-RPA2	Ciccia et al., 2009	N/A
Plasmid: pMSCV-HA-MRE11	Ciccia et al., 2014	N/A
Plasmid: pMSCV-HA-NBS1	Ciccia et al., 2014	N/A
Software and Algorithms		
Prism	GraphPad	https://www.graphpad.com/scientific-software/prism/
ImageJ	National Institutes of Health	https://imagej.nih.gov/ij/
Gatan Micrograph software	Gatan	http://www.gatan.com/products/tem-analysis/gatan-microscopy-suite-software
CometScore Software Version 1.5	TriTek	http://autocomet.com/index.php?id=cometscore
ImageQuant software	GE Healthcare Life Sciences	http://www.gelifesciences.com/webapp/wcs/stores/servlet/catalog/en/GELifeSciences-us/applications/image-analysis-software/
R 3.4.1	The R project for statistical computing	https://www.r-project.org
Cell Profiler 2.2.0	Broad Institute	http://cellprofiler.org
Other		
Stratalinker with monochromatic 365 nm lamps	Stratagene	N/A
FEI Tecnai 12 EM microscope	FEI	N/A
GATAN high-resolution camera	Gatan	N/A
Nikon Eclipse 50i	Nikon	N/A
BX61TRF Olympus microscope	Olympus	N/A
Leica GSL scanner	Leica	N/A
Typhoon FLA9500	GE Healthcare	N/A
JL Shepherd Mark I cesium irradiator	JL Shepherd & Associates	N/A